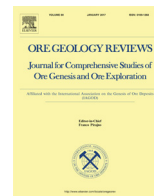




Contents lists available at ScienceDirect

Ore Geology Reviews

journal homepage: www.elsevier.com/locate/oregeo

Thermomechanical erosion of ore-hosting embayments beneath komatiite lava channels: Textural evidence from Kambalda, Western Australia

Sebastian Staude^{a,*}, Stephen J. Barnes^b, Margaux Le Vaillant^b

^a Maylands, WA 6051, Australia

^b CSIRO Mineral Resources, Kensington, WA 6151, Australia

ARTICLE INFO

Article history:

Received 10 December 2016

Received in revised form 16 March 2017

Accepted 2 May 2017

Available online xxx

Keywords:

Thermomechanical erosion

Komatiite

Magmatic Ni-Cu-(PGE) deposit

Embayment

Pinchout

Kambalda

ABSTRACT

Archean komatiite-hosted nickel deposits at Kambalda, Western Australia, are located in embayments within channelized lava flows. The origin of these embayments is controversial. The currently favoured model invokes pre-existing topographic features filled in by the komatiite and sulfide melt and subsequently modified by thermomechanical erosion. New evidence from sulfide deposits on the eastern limb of the Kambalda Dome includes well preserved magmatic textural relationships of the sulfides with the surrounding rocks suggesting the entire embayment was formed by thermomechanical erosion. These textures are particularly well preserved within the Moran deposit of the Long-Victor Complex which lacks the younger intense structural deformation that other Kambalda deposits have undergone. The vestiges of an older, broad concave embayment are represented by sediment-sulfide textures present on the flanks up to 150 m away from the younger steep-sided embayment. Sediment-sulfide contacts are marked here by a globular silicate-sulfide intergrowth, interpreted as emulsion, and cumulate-like mono-sulfide solid-solution (MSS) grains surrounded by interstitial silicate melt. Textures preserved from the formation of a steep-sided embayment are frozen into the basalt-sulfide contact and include an undulating contact with sulfide-filled microfractures and a ferrichromite layer, basalt-sulfide breccia and interpreted crystallized silicate-sulfide liquid emulsions and basalt plumes rising into the sulfides. Textures from the last step of embayment formation are found in the pinchouts, i.e. where the massive sulfide ore is bounded top and bottom by basalt. They include the same textures that were formed during the excavation of the steep-sided embayment but they also feature interpreted basalt-sulfide emulsions on the upper contact, cm-scale silicate-sulfide-ferrichromite layering on the upper contact, and a vesicular basalt “scum layer” floating on the sulfides beneath the solid older basalt.

All these textures represent frozen examples of different stages during the excavation and formation of the embayment, and reflect physical processes responsible for thermomechanical erosion. The initial disposition and orientation of ore-hosting channels was controlled by paleo-topography, probably defined by syn-volcanic faults, but the textures we describe show that within the channel the geometry of the entire embayment was the product of erosion. The sulfide melt itself played a major role in the process owing to its high density, high heat content and very low viscosity, but the hydrated nature of the underlying altered basalt was also critical. Fluids were released from the basalt due to the high temperature in the 1–2 cm immediately beneath the sulfide melt with instant flash boiling creating a network of microfractures. Pre-existing fracture networks and breccia in the basalt allowed the sulfide melt to locally infiltrate the substrate to a greater depth increasing the hydraulic head at the tip of the fracture, thus accelerating the erosion process. Once a critical sulfide melt thickness is reached, partly aided by a growing pile of matrix (net-textured) sulfides, the pressure difference on the embayment floor compared to the basalt at the bottom edges of the embayment becomes high enough to allow the liquid sulfides to melt sideways to form a pinchout.

© 2017 Elsevier B.V. All rights reserved.

1. Introduction

Nickel deposits at Kambalda (Western Australia) are the type example for magmatic sulfides found on the basal contacts of

* Corresponding author.

E-mail address: sebastian.staude@yahoo.com (S. Staude).

channelized komatiite lava flows (Gresham and Loftus-Hills, 1981; Leshner et al., 1984; Cowden, 1988; Leshner, 1989; Cowden and Roberts, 1990; Beresford et al., 2002, 2005; Barnes, 2006a; Barnes et al., 2013). Within the lava channels, sulfides accumulated in linear trough-shaped embayments on the top surface of the footwall basalt. The margins of these embayments are commonly marked by “pinchouts”, where sulfides are hosted by basalts beneath and above.

The origin of the embayments has been debated since the discovery of the Kambalda deposits in 1966. They have been variously interpreted as trenches produced by magmatic thermomechanical erosion by the komatiite lava (Huppert and Sparks, 1985), purely structural features generated by folding and thrusting (Stone and Archibald, 2004; Stone et al., 2005), syn-volcanic grabens (Brown et al., 1999), pre-volcanic topography (Gresham and Loftus-Hills, 1981; Squire et al., 1998) or pre-volcanic topography locally modified by volcanic erosion (Leshner et al., 1984; Leshner, 1989; Williams et al., 1998). The debate has been motivated by a shortage of direct field evidence for thermomechanical erosion around the Kambalda orebodies (Leshner, 1989; Squire et al., 1998). However, a body of such evidence is gradually growing. Evans et al. (1989) mapped transgressive relationships between massive ores and underlying basalts that implied a primary erosional trench about 5 m deep at the Foster deposit. Frost and Groves (1989b) reported accumulation of ocellar textured “xenomelts” derived from molten sediment that had accumulated at the top of the basal komatiite flow on the flank of the Fisher shoot. Staude et al. (2016) provided field evidence for pinchouts in the Moran deposit being the result of lateral thermal erosion by the sulfide melt itself, based on textures found on the basal basalt-sulfide and the upper sulfide-basalt contacts, consistent with observations made at Jan and Juan shoots on primary undisturbed contacts in pinchouts (Leshner, 1983, 1989; Leshner and Barnes, 2009).

The substrate erosion model is now widely accepted for most komatiite-associated deposits, with compelling evidence for erosional contacts beneath contact massive sulfide ores reported from a number of deposits, e.g. Silver Swan in the Kalgoorlie Terrain of Western Australia (Dowling et al., 2004); Digger Rocks in the Forrestania Belt of Western Australia (Perring et al., 1995), Alexo in the Abitibi Belt, Ontario (Houle et al., 2012) and Katinniq in the Cape Smith (Raglan) Belt, Quebec (Leshner, 2007). However, at Kambalda the evidence is still contentious. Leshner (1989) and Squire et al. (1998) argue that basal contacts between massive ores and basalts are for the most part located on unmelted original basalt flow tops, and that the morphology of the embayments is a primary constructional feature only locally modified by thermal erosion. In this view, only the sulfidic sediment originally present between the basalt and the basal komatiite flow has been eroded. This was supported by modelling of thermomechanical erosion rates for different footwall rocks, showing that siliceous sedimentary rocks or felsic volcanic substrates could be eroded by komatiites at sufficient rates whereas the basalt substrate could not (Williams et al., 1998, 2001). Rice and Moore (2001) argued that thermal erosion at the base of Kambalda flows was not possible. Cas and Beresford (2001) following Cas et al. (1999) argued that komatiite flows would be emplaced under laminar rather than turbulent conditions and hence that the removal of sediment from the base of the embayments was primarily mechanical. Countering this view is the direct observation of thermal erosion in real time at the base of basaltic lava tubes during the Kilauea eruption of Kilauea (Kauahikaua et al., 1998). The current view is that thermomechanical erosion and assimilation of sulfide footwall rocks is the favoured genetic model for this class of deposit, but the extent to which ore-hosting embayments are formed by this process remains open to debate.

Excellent underground exposure in the Long-Victor Complex on the eastern limb of the Kambalda Dome reveals evidence for thermomechanical erosion within and outside the komatiite lava channel. The investigated deposits are part of an area that is structurally less complex than other described deposits in Kambalda. Some of these textures are characteristic of certain rock types interacting with the sulfide melt and of particular locations within the lava flow system. These observations not only provide evidence for a thermomechanical origin of the 40 m deep Moran embayment and its associated pinchouts, but also provide some fundamental insights into the physical mechanisms of the erosion process.

In this contribution we expand on our previous work (Staude et al., 2016) which focused specifically on establishing a magmatic origin for the pinch-out structures at the edges of the Moran embayment. Here we describe the textures found on contacts around massive sulfides more generally throughout the Moran and McLeay embayments, and also at ore-sediment contacts on the flanks at Moran, to make a case for a predominantly erosional control on the final morphology of the ore-hosting embayments. We interpret the contact textures as products of melting-infiltration fronts, whereby footwall melting is enhanced by physical infiltration of superheated sulfide liquid into hydrofractures. This potentially self-reinforcing process may be active in the formation of sulfide-hosting embayments and footwall injections in a variety of different magmatic Ni-Cu deposits.

2. Geological setting

2.1. The Kambalda Dome

Nickel deposits associated with channelized lava flows of the Silver Lake Komatiite are found in Kambalda around the Kambalda Dome (Fig. 1), at the St. Ives Group 20 km south of Kambalda, and at Tramways 40 km south of Kambalda (Gresham and Loftus-Hills, 1981; Marston, 1984). Rocks of the Kambalda Dome and adjacent southern areas are situated in the 2.7 Ga old Kalgoorlie Terrain of the Yilgarn Craton (Swager et al., 1997; Goscombe et al., 2009). The tholeiitic Lunnon Basalt forms the basal unit of the entire stratigraphy and is the immediate footwall of the Ni deposits, which typically consist of massive sulfide ores overlain by matrix (net-textured) ores. The basalt is overlain by up to 10 m of sedimentary rocks (Bavinton and Keays, 1978; Bavinton, 1981). Two major types are distinguished. Chlorite-rich sedimentary rocks that are interpreted as derived from erosion of the basalt (or of komatiite if found between sheeted komatiite lava flows) and pyrrhotite-bearing cherts interpreted to be of chemical and volcanoclastic origin (Bavinton, 1981; Beresford and Cas, 2001). The sedimentary rocks are overlain by the lower komatiite unit (Silver Lake Komatiite) which hosts the sulfide deposits at the basal contact of the basal komatiite lava flow. The komatiite forms thin sheeted lava flows above the sediments or, where channelized, form thick (up to 150 m) lava channels or tubes. Beneath the lava channels sedimentary rocks present elsewhere at the basal contact are absent (Gresham and Loftus-Hills, 1981; Leshner, 1989). The upper komatiite unit (Tripod Hill Komatiite) is composed of thin sheeted lava flows (Thomson, 1989) and does not contain economic sulfide mineralization. The komatiite is overlain by the Devon Consols and Paringa basalts and younger volcanoclastic rocks. The whole sequence has been metamorphosed to upper greenschist to lower amphibolite facies. It has also been intruded by felsic to intermediate magma forming a trondhjemitic intrusion in the centre of the Kambalda Dome as well as several mafic to felsic dykes and sills. Despite the younger metamorphic overprint many primary volcanic textures are preserved in the basalt and komatiite and hence the prefix “meta-” is omitted.

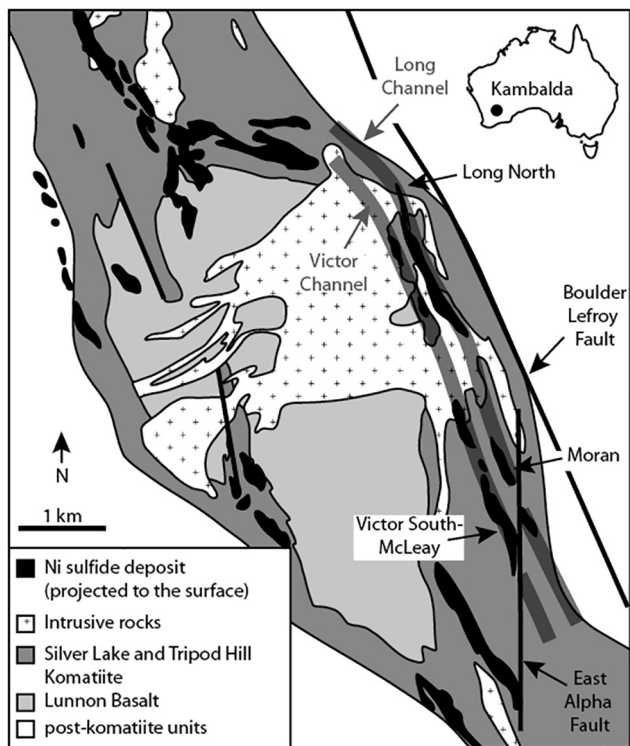


Fig. 1. Simplified geological map of the Kambalda Dome and its Fe-Ni-Cu sulfide deposits (projected to the surface) after Gresham and Loftus-Hills (1981), Marston (1984), Staude et al. (in press). The Long North, Moran and Victor South-McLeay deposits are part of the Long and Victor channels, respectively, on the eastern limb of the Kambalda Dome.

The basal komatiite lava flow of the Silver Lake Komatiite hosts the Ni deposits in channelized parts of the lava flows. These channels can be traced for tens of km (Marston, 1984), and intermittently contain embayments of various depth hosting the sulfide deposits. Embayments are locally also referred to as troughs, but due to its frequent use of this term in the past to denote tectonic structures we follow the suggestion by Cas and Beresford (2001) to restrict the term trough to structural features. We use the term “embayment” as a purely descriptive non-interpretive term. Most embayments have steep sided walls, a flat floor and pinchouts surrounding the base although broad concave embayments are also known (Leshner and Barnes, 2009).

Five to six sub-parallel komatiite lava channels are known around the Kambalda Dome. Although slightly undulating they are not strongly meandering as observed for example in the Katinic deposit of the Raglan Belt in Canada (Williams et al., 2011). To the west the komatiite units thin to less than 100 m in thickness and no further lava channels are known (Gresham and Loftus-Hills, 1981; Marston, 1984). To the east the total komatiite thickness reaches 1 km before being truncated by the Boulder-Lefroy Fault (Fig. 1) and diamond drilling and downhole electromagnetic surveys did not identify further komatiite lava channels within 1 km of the easternmost known channel (Long channel; Staude et al., in press).

Most sulfide deposits are found on the base of embayments (approximately 80%; Gresham and Loftus-Hills, 1981) with a characteristic profile where massive sulfides overlay the basalt and are followed by matrix sulfides and barren komatiite (open contact sulfides) or in pinchouts where massive sulfides are in contact with older basalt beneath and above (pinchout sulfides). In some cases Ni-bearing sulfides are found on sedimentary rocks on the flanks next to the embayment. Most sulfide deposits in Kambalda are

highly overprinted by metamorphism, younger faults, and magmatic dykes creating multiple ore lenses within single deposits, cm-scale separation of pyrrhotite and pentlandite forming a foliation of the ore and mechanical remobilization of sulfides into surrounding rocks.

All Ni deposits on the eastern limb of the Kambalda Dome are mined as the Long-Victor Complex where two mineralized channels are found (Fig. 1). The western Victor channel hosts the Gibb, Gibb South, Victor, and Victor South-McLeay deposits all of which are of high Ni tenor (where tenor denotes the Ni content of the sulfide component) of 12–16% Ni. The eastern Long channel hosts the Long North, Long, Moran and Moran South deposits and mineralization all of which are of medium Ni tenor, between 10% and 14% Ni (Staude et al., in press). Samples for this study were collected from the Long North and Moran deposits within the Long channel and from the Victor South-McLeay deposit within the Victor channel. This contribution reports observations on underground exposures of all these orebodies, but concentrates on Moran due to its well-preserved nature and its nearly complete accessibility in underground workings over the whole orebody between 2011 and 2016.

2.2. Deposit geology – Long North

Long North is part of the Long embayment within the Long channel but is displaced eastwards by younger conjugating fault sets from Long (Staude et al., in press). A trondhjemite intrusion forms the footwall in large areas and numerous felsic to intermediate dykes crosscut the stratigraphy resulting in truncated lenses of mineralization being preserved. Widespread pyrite-chalcopyrite, magnetite or millerite alteration of massive sulfides destroyed most primary magmatic textures; however, where basalt forms the footwall the mineralized lenses contain primary magmatic sulfide-basalt and sulfide-komatiite contacts.

2.3. Deposit geology – Moran

The Moran deposit is situated on the eastern flank of the Kambalda Dome within the Long komatiite channel of medium Ni-tenor south of the Long deposit (Staude et al., 2016, in press). The deposit is situated in an embayment that is up to 40 m deep in relation to the sheeted komatiite lava flows on the flank of Moran (Figs. 2 and 3). The elliptical orebody is completely surrounded by a pinchout which was described in more detail by Staude et al. (2016). The basal floor of the orebody is gently undulating on small scale but nearly planar on a deposit scale. Towards the south however, the edges of the embayment are deeper in comparison to the centre (Figs. 3d and e). The pinchout geometry is also more complex in the south exhibiting multiple small barren pinchouts on the western margin above the sulfides (e.g. Fig. 3d) or a double sulfide-filled pinchout on the eastern margin (Fig. 3e). The overall geometry changes from a nearly symmetrical steep sided embayment in the north (Fig. 3c) to a more gently dipping and wider embayment with a more irregular contact to the surrounding basalt in the south (Figs. 3d and e). The base of the embayment does not coincide with a flow-top or a paleo-surface and instead is underlain by pillowed basalt, flow-top breccia basalt, and aphanitic basalt as shown in Fig. 2 where diamond drill hole intersects of the immediate footwall basalt are displayed.

Spinifex-textured komatiite above Moran representing the top of the basal flow indicates a flow thickness of about 90 m above the centre of the deposit. Due to the drill density around Moran and the Cap Fault above the northern part of Moran, this spinifex-textured flow top is only known along the B-B' profile above its centre (Fig. 3b).

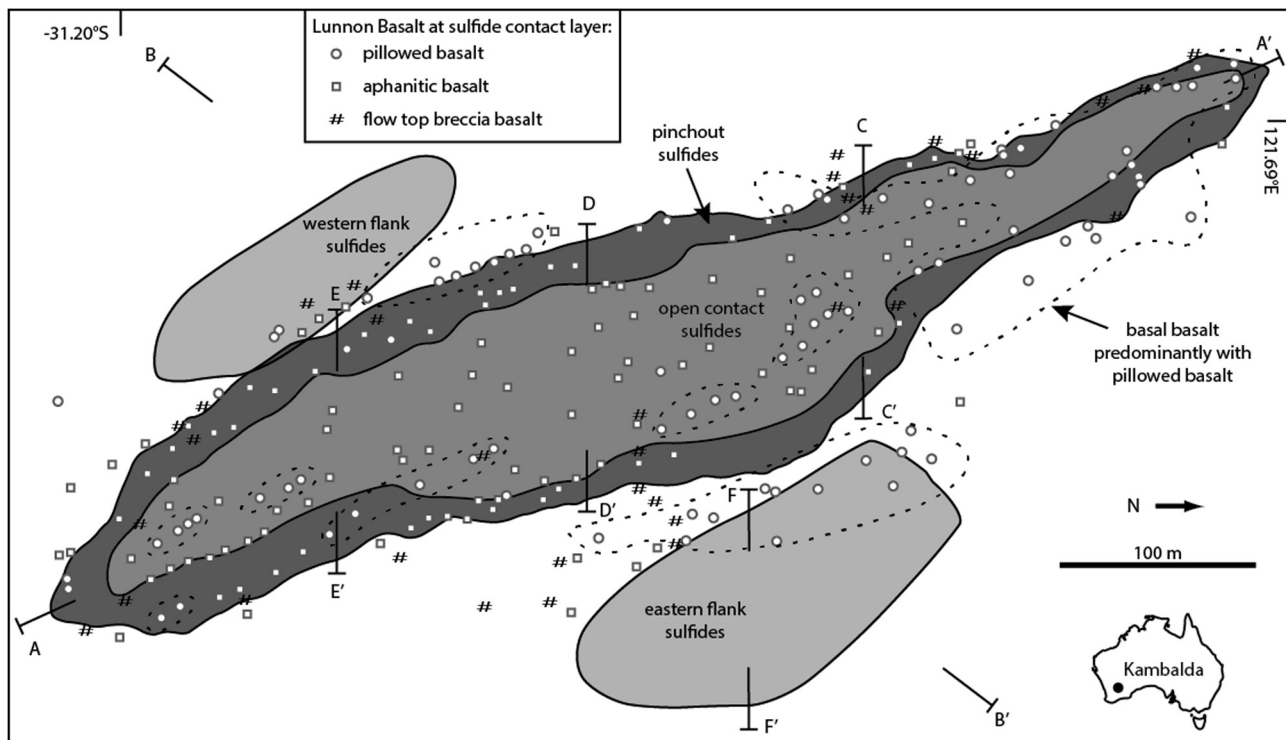


Fig. 2. Plan view of the Moran deposit (projected to horizontal plane of footwall contact) showing the elliptical pinchout that surrounds Moran entirely and the satellite flank sulfides of low Ni tenor. Points represent drill hole intersects displaying the nature of the basal footwall basalt. The location of profiles presented in Figs. 3 and 10 are displayed here.

In the centre of the orebody massive sulfides reach 20 cm in thickness with a Ni tenor of approximately 16% gradually increasing in thickness from the centre to the sides of the embayment to a maximum of 4 m in the pinchout with a Ni tenor of 12–13%. The massive sulfides are sharply overlain by matrix sulfides everywhere outside the pinchouts. Matrix sulfides reach up to 5 m in the centre of the ore body and gradually thin to only a few cm before the pinchout. No matrix sulfides are observed in the pinchout. The contact of matrix sulfides to the overlain barren komatiite is sharp.

The largest proportion of Moran sulfides is found at the base of the embayment; however, there is some uneconomic satellite mineralization on the flanks to the west and east (Fig. 2) and to the north in isolated patches within the Long channel. These flanking sulfides are found in 10–30 m thick sheet-flow facies komatiites (Barnes, 2006b) and are characterized by thin (<1 m) massive sulfides and the lack of matrix sulfides. Close to Moran massive sulfides with a Ni tenor of 10–12% overlie the basalt. Further away sulfides overlie sediments and the Ni tenor gradually decreases to 5–6%. No Ni-bearing sulfides are observed more than 150 m away from the Moran main orebody.

Compared to other deposits in Kambalda, Moran is crosscut only in a few places by younger magmatic dykes and sills and there are no faults interacting with the orebody. The hanging-wall of the deposit is composed of serpentinized komatiite and only occasionally of the talc-magnesite assemblage that usually destroys any primary textures in neighbouring deposits. Metamorphism caused a foliation within massive sulfides creating bands of pentlandite alternating with pyrrhotite. Regularly up to 10 cm large pyrrhotite-free sigma-shaped porphyroblasts are observed in the massive sulfides. They are composed of chalcopyrite-pyrite symplectite with grain sizes of 5–50 μm . The banding of pentlandite is continuous through these porphyroblasts.

Due to the well preserved nature of Moran many different magmatic textures on basalt-sulfide and sediment-sulfide contacts can be observed.

2.4. Deposit geology – Victor South-McLeay

The Victor South-McLeay deposit is part of the high Ni tenor Victor channel and is located south of Victor and west of Moran (Fig. 1). The deposit is displaced by several N-S and E-W trending faults creating several ore surfaces (the northern ones are known as Victor South and the southern ones as McLeay) that are remobilized. Sulfides are found in sheared open contact surfaces, as mobilized sulfides hosted by komatiite and are also found up to 150 m into the footwall basalt. In non-faulted ore surfaces primary magmatic textures are preserved. The western termination of the orebody is situated in a pinchout whereas in the east no pinchout is observed, although here structural overprints complicate the geological interpretation. Frequent E-W striking felsic dykes and flat sills cut through Victor South-McLeay.

In large areas of McLeay, barren komatiite of up to 1 m in thickness is situated between the massive and matrix sulfides. Often, this is accompanied by spinifex-textured olivine on the contact of massive sulfides to the barren komatiite above (Staude et al., in press). This relationship is different to spinifex observed with massive sulfides from Coronet and Lunnon (Groves et al., 1986; Barnes et al., 2016a,b) and its origin is still under debate.

3. Analytical procedures

3.1. 2D and 3D X-ray imaging

The cm-scale element maps in this study were generated by desktop microbeam XRF at the CSIRO ARRC facility, Perth,

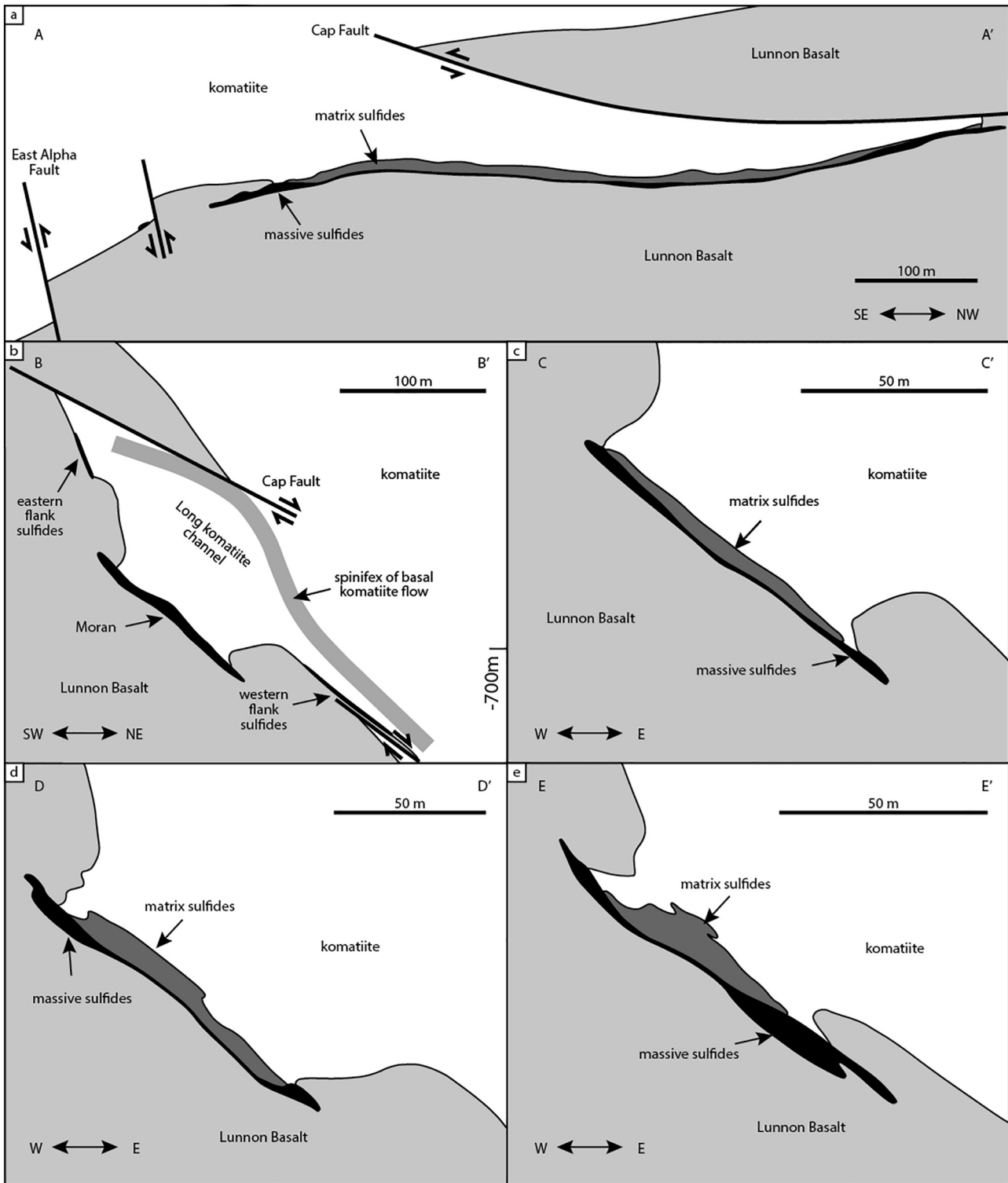


Fig. 3. (A) NNW-SSE profile through the Moran deposit along the channel flow direction. (B) SW-NE profile through Moran showing the overall geometry of the Long channel hosting the Moran embayment and the basal flow top indicated by spinifex-textured komatiite. (C–E) E–W profiles from north to south through Moran showing the contact relations within the embayment of massive sulfides in pinchouts and matrix and massive sulfides in open contacts.

(Barnes et al., 2016a,b). Maps were collected with the Bruker Tornado™ desktop unit equipped with a rhodium target X-ray tube operating at 50 kV and 500 nA without filters and an XFlashVR silicon drift X-ray detector. Maps were created using a 25 μm spot size on a 25–40 μm raster with dwell times of 10 ms per pixel.

Maps are represented as un-quantified background-corrected peak height data for K α peaks for each element.

3D images of hand samples were collected using medical XCT scanning technology, on decimetre scale samples with coarse sulfide aggregates (Godel et al., 2006; Robertson et al., 2015). The

Medical X-ray Computed Tomography system used for this study is a SOMATON Definition AS Medical CT Scanner. This instrument is composed of a rotating X-ray source producing a fan-shaped X-ray beam, along with a rotating set of X-ray detectors (Multislice UFC™ detectors), and a 100 kW generator. The X-ray source is fitted with an STRATON MX P High Performance CT-X-ray tube, with intensity and voltage ranging from 20 to 800 mA and from 70 to 140 kV, allowing the X-ray to be transmitted through dense and complex material such as disseminated to blebby magmatic Fe-Ni-Cu sulfides. Reconstruction to produce the tomographic dataset was done on the Syngo® Acquisition Workspace, and involves correction for anisotropic voxel sizes. Data used for this study were collected using the following 120 kV and 571 mA as set up, using the sequential mode with a 0.6 mm spacing between slices. Pixel size vary between samples from 209 to 429 μm (mainly around 220–250 μm).

4. Results

4.1. Contact relationships at massive sulfide margins

Textures occurring between massive sulfides and the surrounding silicate rock vary depending on the location and the lithological contact. Textures on the basal basalt contact differ from textures observed on the basal sediment contact, on the upper pinch-out contact, and on the contact of sulfides to the matrix

sulfide-hosting komatiite above. All textures observed contain dendritic to skeletal ferrichromite, except contacts involving sedimentary rocks.

4.1.1. Basal basalt-sulfide contacts

Two mutually gradational types of sulfide-footwall interaction have been observed on non-tectonized contacts between massive ore and underlying basalt. The first takes the form of locally plumose contacts (Figs. 4a, b, and 5), and the second comprises zones of sulfides cementing underlying brecciated basalt (Figs. 4c and d). Both contact types are associated with development of distinctive growth of ferrichromite.

The most frequently observed contact relationship between footwall basalt and the sulfides was described in detail by Staude et al. (2016). A few-cm thick layer consists of intimately intermixed silicate and sulfide, where silicate forms irregular mushroom-shaped or globular protrusions extending upward from the underlying basalt (Figs. 4b and 5a, b, c, f). To avoid genetic terminology, we refer to this layer as “plumose inclusion ore”. This texture is observed in all sulfide deposits of the eastern limb of the Kambalda Dome, where the contact is not obscured by shearing. Similar textures have also been reported from Lunnon (Kambalda; Ewers and Hudson, 1972), Perseverance (formerly known as Agnew; Western Australia, Barnes et al., 1988), Katinni (Canada; Lesher, 2007) and Alexo (Canada, Houle et al., 2012). A 1–3 cm thick band of sulfide-filled microfractures of less than

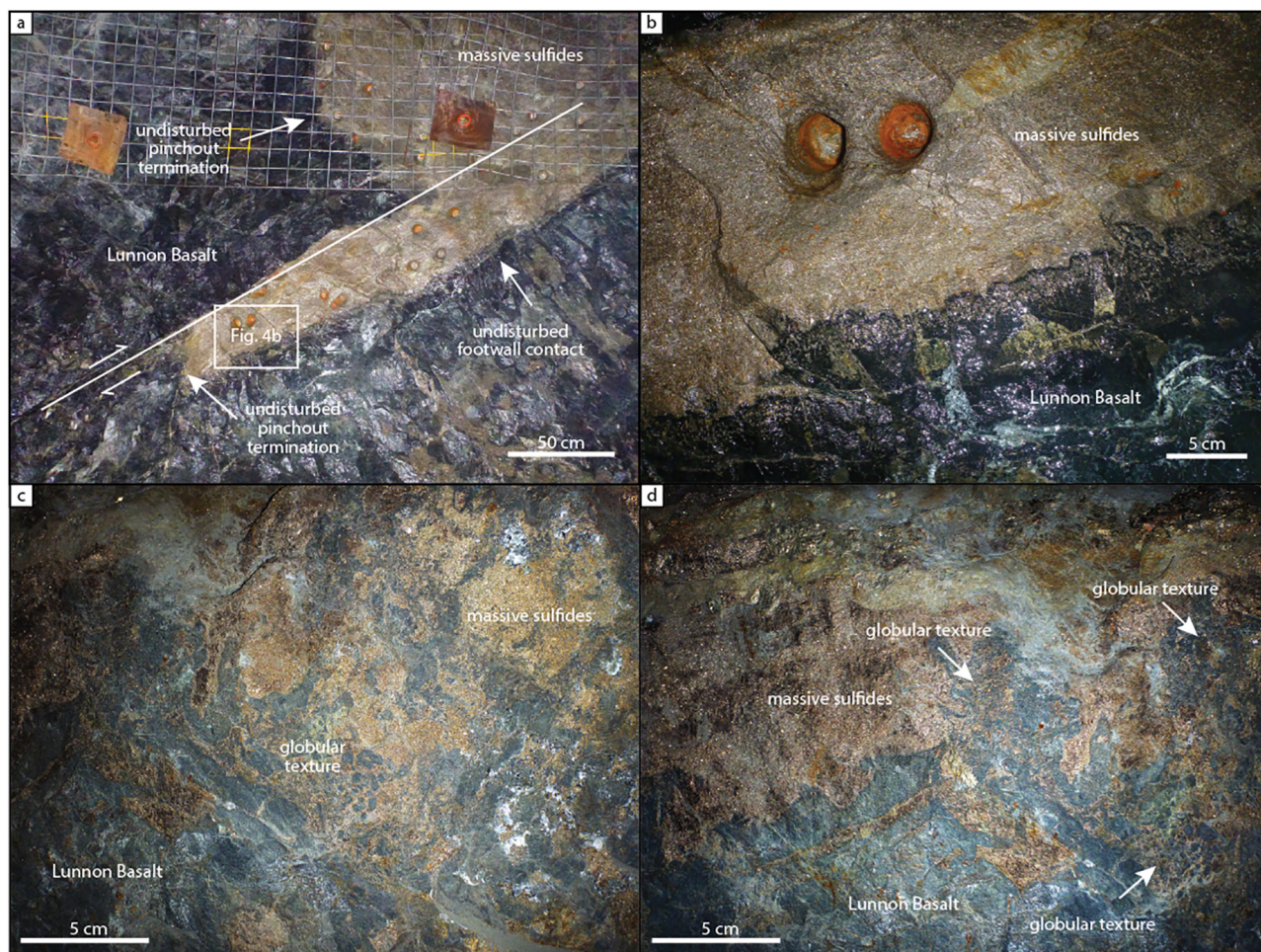


Fig. 4. (A) Photographs of the eastern pinchout termination of Moran. (B) Close up of (A); white box, showing the undulating nature and the basalt-sulfide textures of the basal contact. (C and D) basal basalt-sulfide contact of Victor South-McLeay showing brecciation of basalt accompanied by the formation of sulfide-silicate emulsions (globular texture).

1 mm in thickness for each fracture (Figs. 4b and 5) or sulfide globules of up to 5 mm in diameter for each globule (Fig. 2e in Staude et al., 2016) is developed parallel to the contact, in some cases with internal parallel sulfide-rich sub-layers and/or sub-parallel veins extending into the basalt (Figs. 4a, b, and 5d, e). Based on microscopy the silicate portion within the microfracture layer is composed of coarse grained silicates (mainly amphibole and plagioclase) if in contact with sulfides and of aphanitic

fine-grained domains where sulfides are absent (see Supplementary Fig. 2). A sulfide-free ferrichromite-rich and ilmenite-bearing 1–5 mm thick layer of basalt, interpreted by Staude et al. (2016) as a basalt melt film, is situated between that microfracture-containing layer and the overlying 1–2 cm thick basal sulfide layer containing a network of ferrichromite aggregates. In the example shown in Figs. 5a and b multiple parallel plumose basalt melt film layers are developed within the massive sulfide. In all cases, the

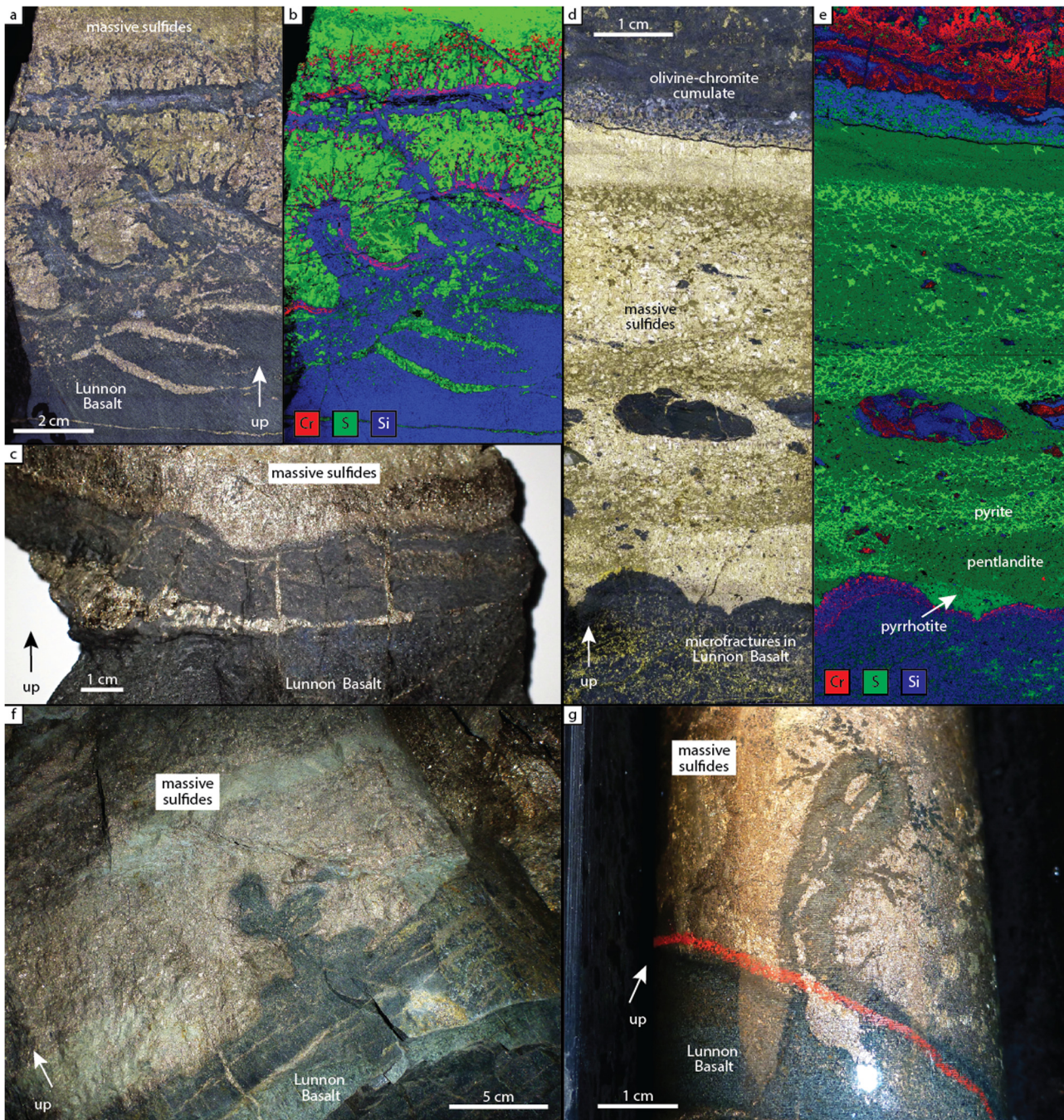


Fig. 5. (A) Photo and (B) chemical map of a basalt plume from the Moran basal basalt-sulfide contact. The upper silicate layer is part of a basalt block still connected to the host basalt about 10 cm away. The basalt plume forms between the basalt and the slab. Note, that chromite on the slab and on the plume forms mainly on the contact facing upwards and represents the sulfide-free basalt melt film discussed in the text. A 3-D medical computed tomography video of moving slices through the sample is shown in the Supplementary material. (C) Hand specimen from the basal basalt-sulfide contact of Moran showing a block of basalt partly connected with the basalt beneath which is accompanied by perpendicular fractures. (D) Photo and (E) chemical map of a polished slab from the Victor South-McLeay deposit. The polished slab include the basal basalt-sulfide contact and the upper sulfide-komatiite (matrix sulfides) contact. Note the microfractures in the upper basalt layer beneath a sulfide-free basalt melt film and the chromite abundance on both contacts. (F) Photo of the basal contact of Victor South-McLeay showing microfractures in the upper basalt layer and a large basalt plume rising into the sulfides. (G) Photo of a diamond core of the Moran basal basalt-sulfide contact showing an exceptionally well preserved basalt plume which is surrounded by chromite. Note the sulfides contained within the centre of the plume.

upper contact of the basalt film and the plumes are decorated with cauliflower-shaped aggregates of chromite crystals. This chromite occurs as 1) fine equant grains within the melt film itself, 2) strongly dendritic grains within the adjacent sulfide; indicative of rapid upward growth from the basalt contact into the sulfide liquid (see also Fig. 2 in Staude et al., 2016), and 3) as coarser euhedral grains. The dendritic and non-dendritic chromites are commonly closely intergrown with blue-green hornblende, in some cases filling interstices within the dendritic grains (see [Supplementary material](#) for detailed photomicrographs). Beneath the sulfide-free ferrichromite-rich layer no chromite has been observed but frequent skeletal ilmenite crystals are found in coarse-grained globular silicate areas within the fine-grained basalt.

The second significant contact type, observed in Victor South-McLeay and in Moran, occurs where massive sulfides overlay brecciated basalt to form sulfide-matrix breccia (i.e. matrix-supported breccias; Barnes et al., 2017a). In such cases, as at the McLeay basal contact illustrated in Figs. 4c and d footwall basalt clasts are cemented by sulfides up to 2–3 m into the footwall and partly form globular basalt inclusions entirely enclosed in sulfides (interpreted as emulsion by Staude et al., 2016). In places the relationship is inverted such that globular sulfide is developed within the basalt globule itself. Further away from the contact the basalt changes from rounded irregular soft-walled inclusions with thin chromite-decorated melt films into completely angular and commonly jigsaw-fit breccia clasts with chromite-free margins where sulfide-filled fractures typically terminate within the clasts (Fig. 6).

Rare textural variants of the basal basalt-sulfide contact found only at Moran comprise a fine-grained sulfide-basalt intergrowth forming enclaves of fine grained basalt, approximately 1 cm in diameter, surrounded by sulfides (Figs. 7a–c). The fine-grained sulfide-basalt intergrowth is inhomogeneous, forming small sulfide-free basalt spheres within the sulfide-basalt intergrowth (Fig. 7c). The exact inverse of this texture is also observed where 2–3 cm sulfide globules are enclosed within a matrix of basalt (Fig. 7d). (Videos of moving slices through 3-D medical computed tomography images of both textures are found in the [Supplementary material](#)). These textures appear similar to textures interpreted as sulfide-silicate liquid emulsions by Frost and Groves (1989a) at the Foster Shoot, although there the silicate component is identified as komatiite and the silicates occur towards the top of the massive sulfide. While it is desirable to avoid genetic terminology as far as possible, for economy of style we are confident that these textures can only be interpreted as physical mixtures of immiscible sulfide and footwall-derived basaltic melt, and consider that use of the term “emulsion texture” is justified.

4.1.2. Upper sulfide-basalt pinchout contact

Textures on the upper pinchout contact have been described in detail by Staude et al. (2016) and comprise a layer or multiple layers of prismatic amphibole oriented long-axis downwards into the sulfides. These crystals are terminated by an intergrowth with skeletal ferrichromite. In some places, an amygdale-rich homogeneous medium-grained basalt layer, up to 30 cm thick, is found between the massive sulfides and the inhomogeneous amygdale-free fine-grained Lunnon Basalt above (Figs. 8a and b). This was interpreted by Staude et al. (2016) as floating vesicular basalt melt, originated from the basal melting of basalt, trapped beneath solid basalt. Due to the large amount of contained amygdaloids and its position at the top of the sulfide layer, this layer was referred to as “basalt scum”. Rarely, the interface between sulfides and this basalt layer is characterized by egg-carton shaped sulfide domes rising into a fine (mm-scale) basalt-sulfide emulsion (Staude et al., 2016) or, more commonly, by alternating 1-cm scale

contact-parallel layers of actinolite crystals with sulfides (Figs. 8c and d). The actinolite-ferrichromite layer and the basalt layers are observed at the upper sulfide-basalt contact in pinchouts of the Victor South-McLeay and Moran deposits.

4.1.3. Basal sediment-sulfide contact

Sulfides overlying sedimentary rocks have been observed beneath sheeted lava flow facies on the flanks of the Moran deposit outside the ore-hosting embayment. The most widespread sediment-sulfide textures are sulfide-silicate globular intergrowths with 1–2 mm grain size (Figs. 9a and b), sulfide-filled microfractures within the more competent silicate layers and 1–2 mm large round grains of sulfide within a silicate matrix (Figs. 9c–f), which was called ‘lace-texture’ in a similar texture from Black Swan (Western Australia) by Dowling et al. (2004). Commonly, clasts of sedimentary rocks are completely enclosed in sulfides and surrounded by the globular texture or sulfide cumulate. Footwall plumose textures and ferrichromite, features common at basalt-sulfide contacts, are characteristically absent at contacts with sedimentary footwall. Minor amounts of Cr are only observed within Cr-bearing biotite surrounding clasts of sedimentary rocks (Fig. 9d). In some examples up to 20 μm euhedral titanite and skeletal magnetite has been observed in the silicate portion of the globular texture. Typically, sphalerite and minor galena are observed in sulfides above the sedimentary rocks, whereas they are rare in sulfides above the basalt footwall. The silicate material of the globular texture shows a bimodal chemistry reflecting the surrounding pelitic compositions. Calcium-poor, aluminous chert layers form coherent blocks, while more Ca-rich, lower Si pelitic layers form fine globular textures with sulfide (Fig. 9b). We interpret this relationship as being due to fine-scale variation in degree of melting: quartz rich layers are relatively refractory and remain solid, while the pelitic interlayers melt to form silicate-sulfide emulsions.

Polished sections show mm-sized spherical sulfide-silicate intergrowth which contain smaller silicate droplets of medium grain size. These bimodal droplets are hosted by fine-grained sediment and are found immediately beneath the contact. Representative backscattered electron images (BSE) and photomicrographs of sediment-sulfide contacts are shown in [Supplementary materials](#).

The eastern flank of Moran shows a gradational change from a basalt footwall close to Moran to a sedimentary footwall further away (Fig. 10a). Chemical maps of Cr of two diamond drill holes intersecting the contact show the abundant skeletal ferrichromite on the basalt-sulfide contact (Figs. 10b and c) compared with the lack of chromite and only traces of Cr on the sediment-sulfide contact (Figs. 10d and e).

4.1.4. Upper sulfide-komatiite contacts

The contact between the sulfides and the komatiite above (mostly represented by matrix sulfides) is, in all deposits, gently undulating and marked by a 1–2 mm thick chromite-magnetite layer which can reach a thickness of 10 cm in some cases. Chromite on the sulfide-komatiite contacts has also been reported from the Lunnon and Foster deposits, Kambalda (Ewers and Hudson, 1972; Ewers et al., 1976; Frost and Groves, 1989a); the Silver Swan orebody at Black Swan (Dowling et al., 2004), Alexo, Ontario (Houle et al., 2012) and elsewhere.

In places, patches of skeletal ferrichromite (Fig. 11) are observed immediately beneath the contact. Two types of chromite with different habits are present, 1) Euhedral ferrichromite, which is in direct contact with 2) a layer of very fine anhedral irregular to dendritic chromite. In rare examples carbonate or sulfide filled amygdaloids or globules are found in the komatiites immediately above the contact with the underlying sulfides (Fig. 11c). These globules probably represent sulfide liquid droplets incorporated

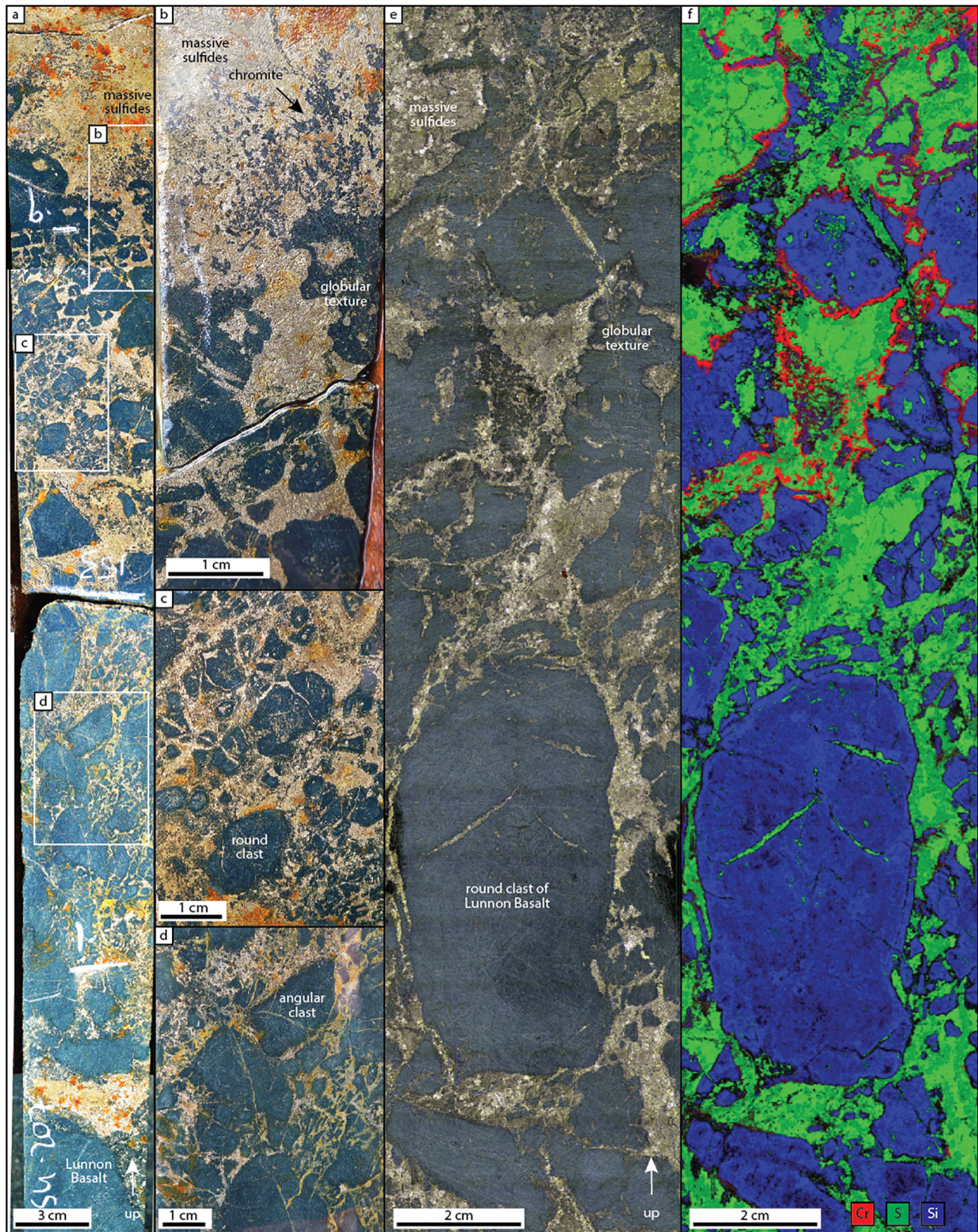


Fig. 6. (A) Diamond drill core photo showing the Moran basal contact of brecciated basalt to sulfides. (B), (C), (D) Close up of (A) to show the gradational change of angular clasts in a jigsaw pattern (D) towards more round clasts (C), basalt-sulfide emulsion and chromite directly on the contact to the sulfides (B). (E) Photo and (F) chemical map of diamond drill core of the Moran basal contact of brecciated aphanitic basalt to sulfides showing the transition from rounded clasts that are partly fractured (bottom) to ferrichromite decorated emulsion (top).

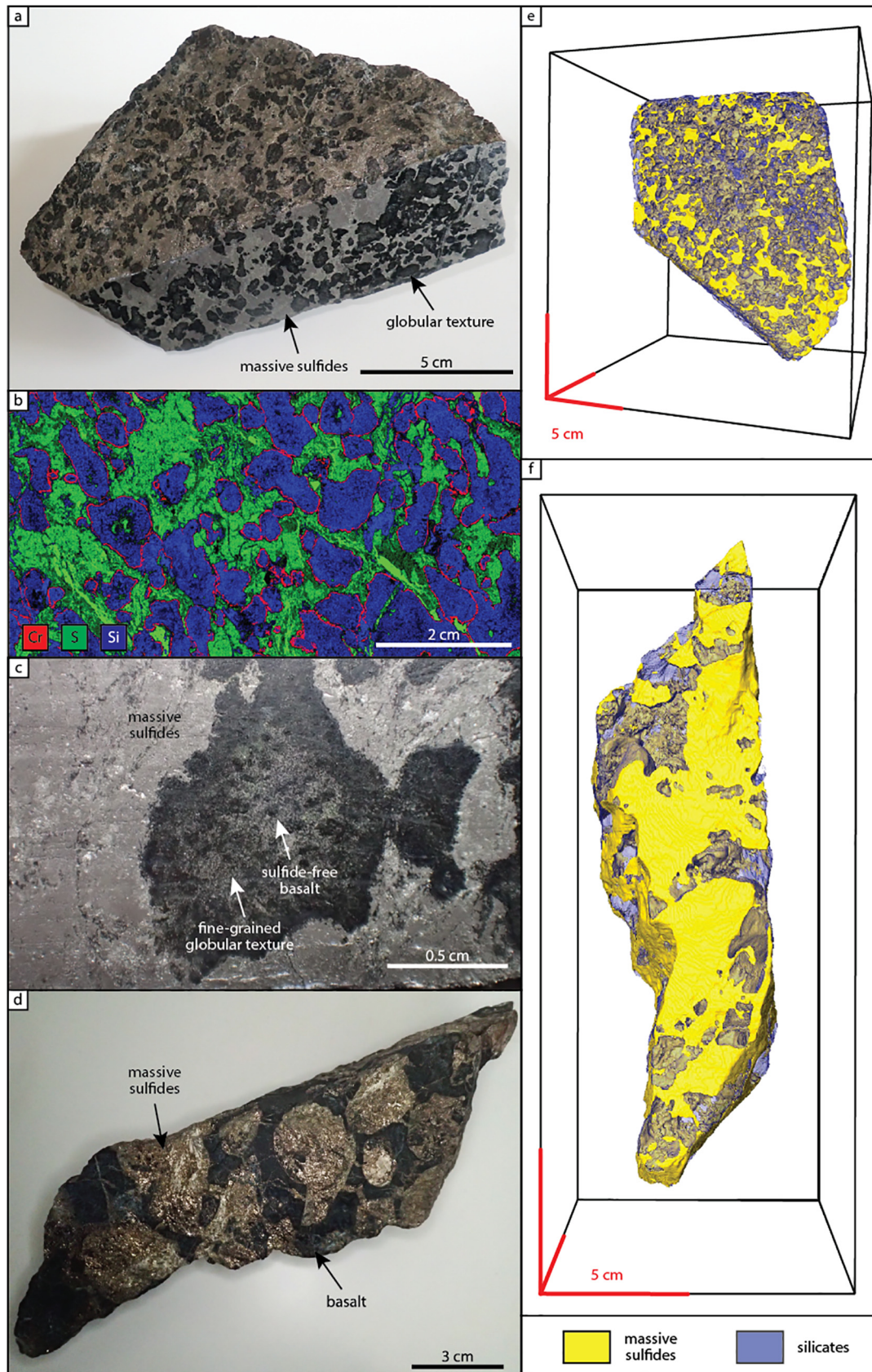


Fig. 7. (A) Hand specimen of a silicate-in-sulfide emulsion from the Moran basal contact. A 3-D medical computed tomography video of moving slices through the sample is shown in the [Supplementary material](#). (B) Chemical map of same specimen. (C) Close-up of one silicate bleb of (A). Note, the bleb itself consists of sulfide-free basalt droplets surrounded by a sulfide-silicate mixture. (D) Hand specimen from the Moran basal contact showing a very coarse sulfide-in-silicate emulsion. (E) 3-D medical computed model of sample shown in (A). (F) 3-D medical computed model of sample shown in (D). The modeled sulfide portion of the sample is shown in yellow and basalt in blue. A 3-D medical computed tomography video of moving slices through the sample is shown in the [Supplementary material](#).

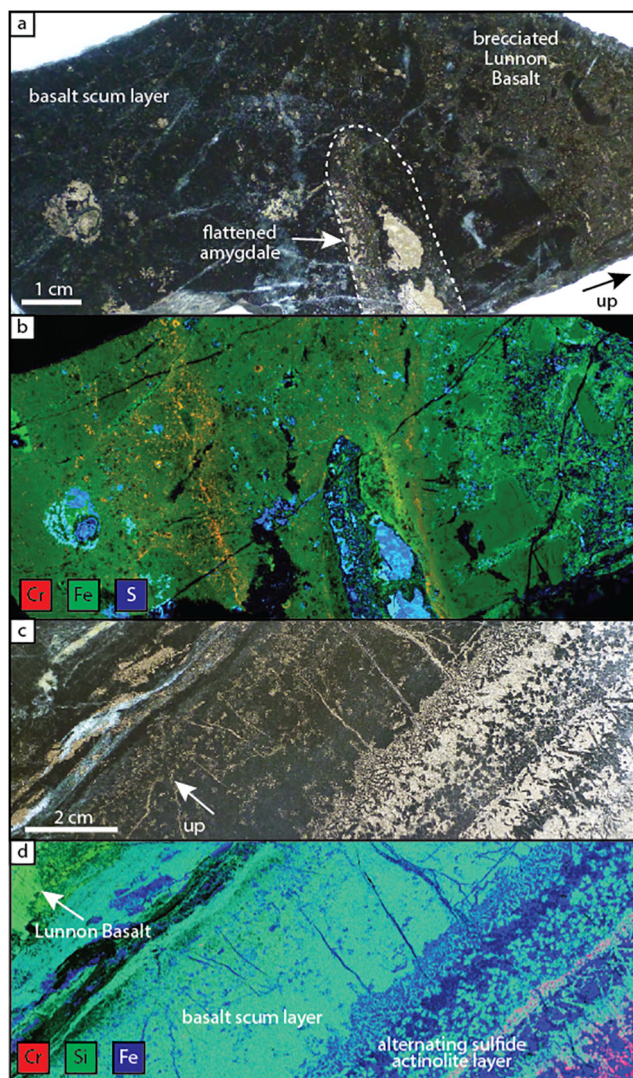


Fig. 8. (A) Photo and (B) chemical map of upper pinchout “scum layer” from Victor South-McLeay. A large amygdale is flattened against the upper brecciated basalt. The breccia infill is a mixture of silicates and sulfides. (C) Polished slap and (D) chemical map of upper pinchout contact from Moran showing alternating layering of actinolite and sulfides, floating basalt scum and unaffected Lunnion Basalt above. Note, the difference in Fe/Si ratios between the basalt “scum layer” and the unaffected Lunnion Basalt and ferrichromite being concentrated on the lowermost actinolite layer only.

into the transporting komatiite magma as a result of attachment to gas bubbles (Mungall et al., 2015) as discussed below.

In parts of Victor South-McLeay the sulfide-komatiite contact is characterized by a layer of plate-spinifex textured olivine hosted by sulfides and is described in Staude et al. (in press). The komatiite immediately above the spinifex is barren. This texture is different from spinifex associated with the hanging-wall sulfide layer of interflow ore in Lunnion and Coronet (Groves et al., 1986; Barnes et al., 2016a) and its origin is still unclear.

5. Discussion

In this section we consider the implications of the textures described above, in terms of the physical processes of sulfide melt emplacement, thermo-mechanical erosion and silicate-sulfide melt emulsion behavior. Some of the detailed textural features provide some intriguing insights into the physics of interactions between molten sulfide and melting silicates.

5.1. Significance of ferrichromite at basalt-sulfide contacts

All primary contacts of sulfide with the surrounding basalt are decorated with dendritic to skeletal ferrichromite, with a composition and growth habit diagnostic of a magmatic rather than metamorphic or hydrothermal origin (Groves et al., 1977; Lesher, 1989; Dowling et al., 2004; Houle et al., 2012; Staude et al., 2016). The detailed distribution in relation to melt films, melt plumes and sulfide-matrix breccias indicates that the presence of chromite is characteristic of co-existence between sulfide and silicate melts. Thus, the footwall basalt must have been molten in immediate contact with the sulfide melt.

5.2. Textures at sediment-sulfide contacts

Textures at sediment-sulfide contacts differ significantly from basalt sulfide contacts. Globular inclusion textures, interpreted as emulsions of silicate and sulfide melts, are observed on every intersected sulfide-sediment contact, and are particularly well developed at cm-scale along original pelitic layers that were less refractory than intercalated silicic cherts (Fig. 9). Evidently the less refractory layers melted and formed emulsions with the sulfide melt, while the Si-rich bands remained as solid xenoliths. The solid cherty slabs and the microfractures within them show that certain layers of the sedimentary package were consolidated when the komatiite erupted whereas other layers were still unconsolidated and formed peperites (Beresford and Cas, 2001).

A particularly informative texture is illustrated in Figs. 9c–f where fine “lace-textured” silicate forms an interstitial film between equant sulfide grains. This texture may be related to the relative melting – solidification temperature ranges of the silicate and sulfide melts. Sediments in Kambalda contain more SiO₂ than the basalt (average 60 wt% (volatile free) in sediments, (Bavinton, 1981), and 49–53 wt% in basalt; Squire et al., 1998) and hence form a higher viscosity melt. The “lace-texture” silicate-sulfide emulsions observed in the Silver Swan deposit formed above a dacite substrate, which also contains a higher content of SiO₂ (median 69.8 wt% SiO₂, Dowling et al., 2004). Si-rich melts have lower solidus temperatures than that of the Ni-rich, Cu-poor sulfide melts at Kambalda and Silver Swan, and hence the silicate melt component would have remained molten over most if not all of the (narrow) solidification range of the sulfide (~1050–1100 °C, based on experimental phase equilibria of Kullerud et al. (1969)). The apparently interstitial “lace-texture” is therefore interpreted as the result of silicate melt being trapped between growing mono-sulfide solid-solution (MSS) crystals, forming what could be considered a type of ‘inverse net-texture’.

5.3. Melt films at basalt-sulfide contacts

The nature of the plumose melt film layers at basalt-sulfide contacts is characteristic of the physical process of thermal erosion. A very similar type of melt film is observed between massive sulfide and interspinifex ore at the Lunnion and Coronet Shoots, Kambalda (Barnes et al., 2016a). There, komatiite melt, displaced by downward migrating sulfide melt, wicks along the silicate-sulfide boundary making a film about 1 cm thick. The presence of molten silicate beneath denser molten sulfide creates a Rayleigh-Taylor instability, from which ascending plumes of amplitudes around 1–2 cm form and detach. At the basalt-sulfide contacts at Moran the microfracture layer, melt films, and chromite layers have a consistent range of thickness between 2 and 5 cm, with plume amplitudes ranging from 1 to 10 cm. Thicker films and larger plumes at the basalt contacts, compared with komatiite contacts in spinifex ore, probably reflect the higher viscosity of the basaltic melt.

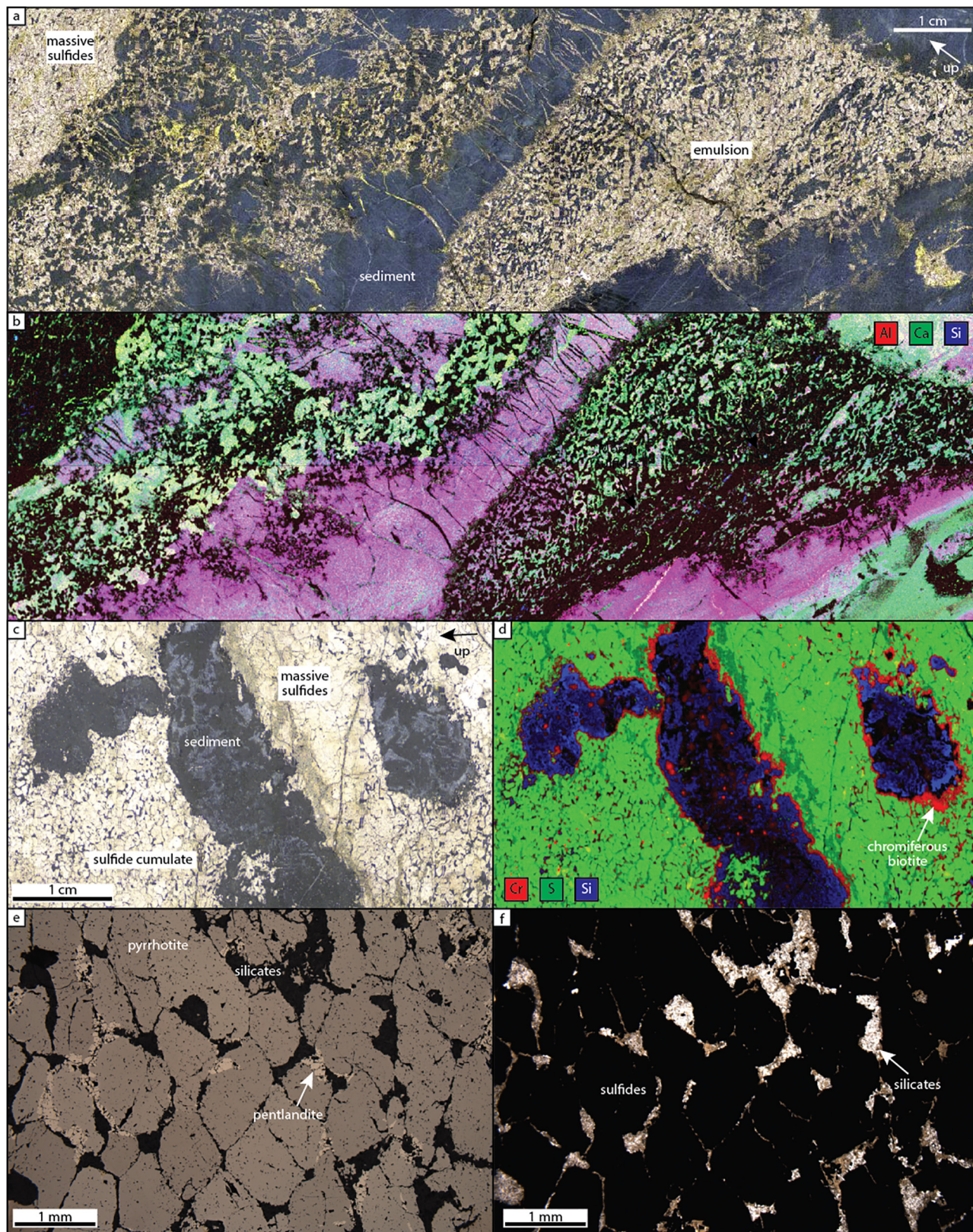


Fig. 9. (A) Photo and (B) chemical map of diamond core of the basal contact from the Moran flank where sulfides overly sedimentary rocks. Note that the silicate portion of the emulsion is bimodal Si- and Al-rich areas. (C) Photo of diamond core and (D) chemical map of same specimen of basal sediment-sulfide contact of the Moran flank. Sulfides form a cumulate of subhedral grains with interstitial silicate. Note, that there is only a weak Cr enrichment on the contact, represented by Cr-bearing biotite. (E) Microphotograph in air under parallel and (F) under cross polarized filters of the sulfide cumulate shown in (C).

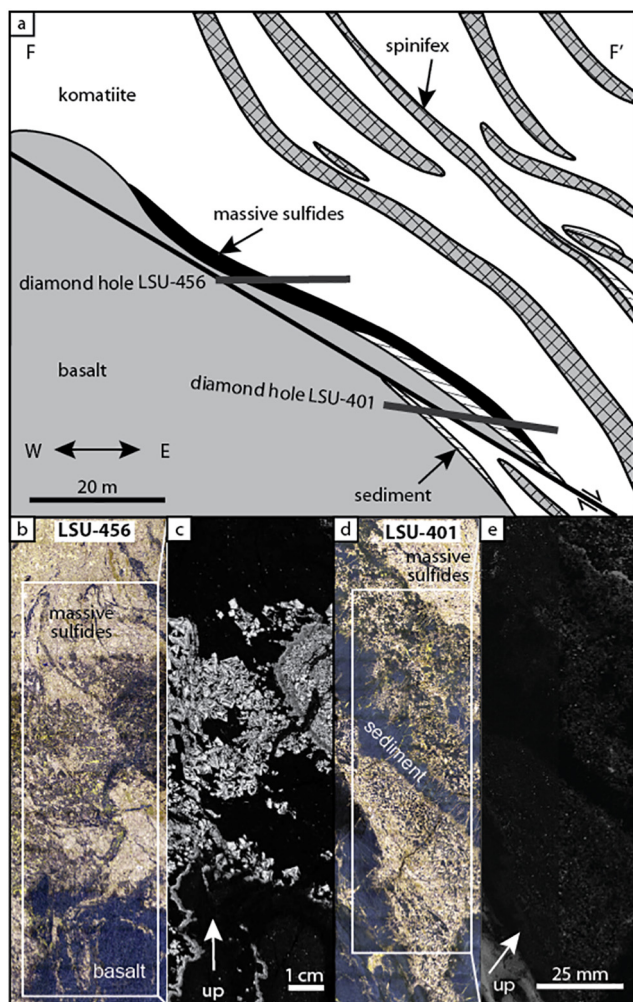


Fig. 10. (A) Profile through the eastern flank mineralization of Moran highlighting the distribution of sediments in relation to massive sulfides and showing the location of diamond holes LSU-401 and LSU-456. No matrix sulfides have been observed in mineralization of the flank. Note, spinifex of the basal flow is less than 10 m from the basal contact in the east, representing sheet flow facies, whereas the flow thickens towards Moran in the west. (B) Photo and (C) chemical map of Cr-concentration of LSU-456 showing the distribution of chromite on the basalt-sulfide basal contact of the eastern flank mineralization. (D) Photo and (E) chemical map of Cr-concentration of LSU-401 showing the lack of chromite on the sediment-sulfide contact of the eastern flank mineralization.

The basaltic melt develops initially as continuous films surrounding completely unmelted basalt. Similar relationships can be recognised at basal sulfide contacts in a variety of different deposits, including elsewhere at Kambalda, indicating that the process observed here is universal and is driven by the physics of melting.

5.4. Footwall breccias and sulfide infiltration

Two major types of sulfide melt infiltration mechanisms into the footwall rocks exist, based on the observed textures as described in Section 4.1.1: 1) Infiltration into pre-existing host-rock fractures and breccias, and 2) infiltration into microfractures. These two textures reflect a different physical process of sulfide melt infiltration which are described in the following paragraphs. Fracture and breccia infill, which produces sulfide-matrix breccia, works on a large scale (metres) but represent isolated features within the embayment. Microfracture infiltration works on a small

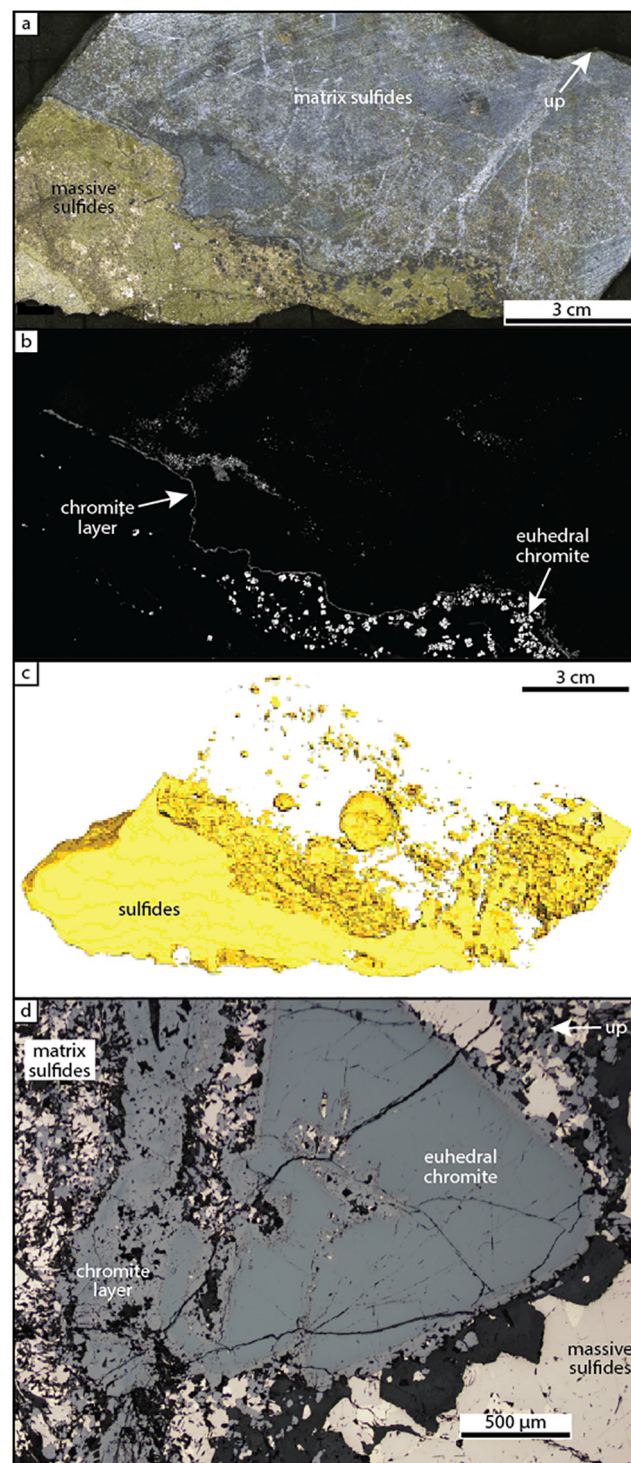


Fig. 11. (A) Polished slab of massive sulfide contact to komatiite (matrix sulfides) above from Long North. Patches of euhedral chromite are concentrated beneath a continuous chromite layer on the contact itself. (B) Photo and (C) chemical map of same specimen showing the distribution of chromite. (C) 3-D model of the sulfides of sample shown in (A) showing blebby sulfides within the matrix portion of the specimen. A 3-D medical computed tomography video of moving slices through the sample is shown in the [Supplementary material](#). (D) Photomicrograph in air of euhedral chromite beneath a continuous layer of dendritic chromite of (A).

scale (millimetres to centimetres) but is effective over the entire embayment and even accompanies type 1 fracture and breccia infiltration.

5.4.1. Infiltration into fractures and breccias

The distinctive transition from fractured basalt with penetrative sulfide-filled veins further away from the massive sulfides to sulfide-matrix breccias with molten and semi-molten basalt close to the massive sulfides highlights the existence of a potentially important mechanism operating during the emplacement of magmatic orebodies.

The Lunnon Basalt contains abundant syn-eruptive breccias, including flow-top autobreccias, pillow breccias, hyaloclastites and inter-pillow splinter-clast breccias (Squire et al., 1998). These breccias are presumably porous and permeable and easily exploited by seawater, by komatiite lavas flowing above them, and particularly by dense sulfide melt.

The distribution of chromite within the sulfide-matrix breccia shown in Fig. 6 is significant for the interpretation of the textures. At the top of the interpreted infiltration zone, the basalt fragments begin to melt following prolonged contact with the substantially superheated sulfide melt. As in the case of the plumose melt films, this melting only happens within a very narrow boundary layer around the solid inclusions, and the so formed silicate melt rises into the sulfide melt and escapes into the overlying komatiite lava flow. The scale of this process is on the order of a few cm, as indicated by the distribution of chromite in the case of sulfide infiltrating spinifex zones of previously solid komatiite flows (Barnes et al., 2016a).

As the column of connected sulfide liquid grows, the excess hydrostatic pressure at its bottom tip increases proportionally, further enhancing the capacity of the sulfide liquid to percolate down through the fracture network (Fig. 12).

5.4.2. Infiltration into microfractures

The presence of a thick chemical sediment between the top of the Lunnon Basalt and the base of the komatiite requires an unknown but long (probably thousands of years) time interval

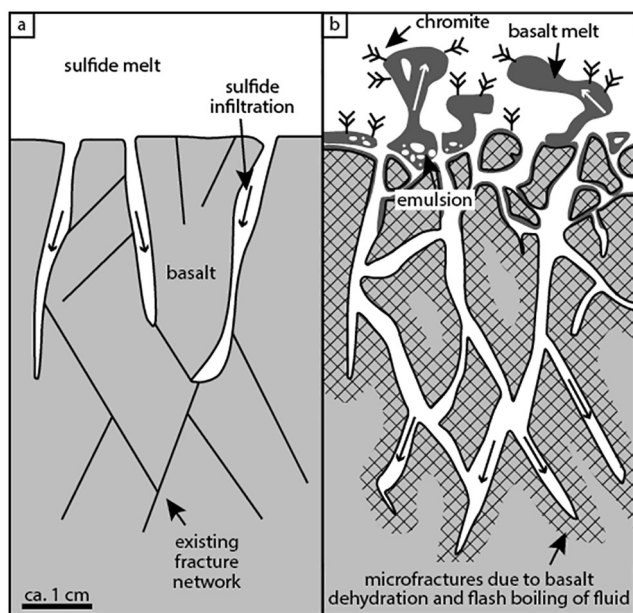


Fig. 12. (A) Cartoon showing the basal basalt-sulfide contact in the embayment. Due to its high density and low viscosity the sulfide melt is able to exploit and infiltrate the existing fracture network creating a sulfide-matrix breccia. (B) Fluids of the hydrated basalt are released due to the high temperature and their flash boiling creates a network of microfractures accelerating the erosion of basalt. Clasts closer to the sulfide melt start to melt. The uppermost basalt clasts are completely molten and form emulsions and plumes. Chromite is growing on the contact between the basalt and sulfide melts.

during which the basalt was exposed to alteration on the sea floor. Roddick (1984) concluded, based on geochemical data, that the Lunnon Basalt underwent an early greenschist facies metamorphism shortly after emplacement due to ocean floor alteration. Seawater infiltrated the cooling fractures and reacted with the basalt to form hydrous alteration assemblages, most likely zeolite-dominated. This would have created a hydrated basalt, with fluids bound in minerals, but also containing unbounded seawater residing in fractures and porosity. When the hot sulfide melt comes into contact with the hydrated basalt the zeolites and other hydrous phases would have broken down, releasing the water. This water, in combination with superheated pore water, rapidly flashes to steam, resulting in sudden increased fluid pressure fracturing the rock beneath the sulfide melt. Therefore, the sulfide melt in combination with water from surrounding rocks could generate additional breccias through hydraulic fracturing, and facilitates its own path into the footwall fracture network.

5.4.3. Infiltration process mechanism

Williams et al. (1998) modeled thermomechanical erosion rates for dry basalt as well as dry and wet and unconsolidated sediments. They assumed an anhydrous basalt substrate but acknowledged that the results are strongly dependent upon the nature and behavior of the substrate (e.g. their water content). Evidence for release of water during thermomechanical erosion was shown by Staude et al. (2016) in the form of a vesicular “scum layer” floating on top of the sulfide melt in the pinchouts of Victor South-McLeay and Moran. The amygdale-rich komatiite, found only in the centre of channelized komatiite lava flows above embayments and previously interpreted as accumulation of fluids due to the crystallization of olivine in prolonged volatile-bearing lava flows (Beresford et al., 2000; Beresford and Cas, 2001), could have originated by the same process, whereby the volatiles of the footwall basalt are released into the overlying komatiite during the thermomechanical erosion process.

Combining conclusions of Williams et al. (1998) with our observations, the fracture infiltration – melting mechanism model shown in Fig. 12, provides a mechanism for generating and deepening erosional channels once the contacts become lined with sulfide melt. Penetration of sulfide melt through the matrix of the breccia provides a mechanism to mechanically detach these fragments from the floor and incorporate them into the sulfide melt. Once enclosed in sulfide melt, the silicate clasts or melt globules are highly buoyant and float rapidly to the top of the sulfide melt (Dowling et al., 2004), where they are either incorporated into the flowing komatiite lava above, or pond beneath the roof of pinchouts to form the vesicular basalt “scum layer” as described in the pinchouts at Moran by Staude et al. (2016). The sulfide liquid in combination with the hydrated basalt hence enhances footwall erosion rates in two ways: by effectively levering silicate material off the floor, and by acting as a highly efficient mechanism for advecting the heat of the overlying flow into the floor on a scale of metres. This process will be many orders of magnitude faster than conductive heat transfer (Robertson et al., 2016). Hence, the position of the melt front at the floor will advance much more rapidly than the conductive isotherms; the melting front proceeds rapidly into completely cold rock (Williams et al., 1998; Gole et al., 2013).

There are two implications. First, as noted by Robertson et al. (2015, 2016), this mechanism precludes derivation of sulfide from the footwall by another mechanism other than direct melting of sulfidic rock. Incorporation of partial melts of footwall rocks is unlikely, as the advancing melting front will rapidly overtake the very narrow boundary layer within the solid rock, where the rock is at a temperature within its melting range; the contact rocks either melt completely, or not at all. Second, this may go some

way to explaining a major paradox at Kambalda about the location of sulfides which are often surrounding the top contacts of pillowed basalt. Whereas thermal erosion provides an explanation for the nature and geometry of the ore-hosting embayments, detailed underground observations by Leshner (1983, 1989) found little evidence (except in pinchouts) for erosional contacts, as discussed further below. Characteristically, the interiors of pillows are much less fractured than the margins. It is likely that if erosion was taking place, the eroding lava would be exploiting fractured and brecciated zones at the margin of cooling units, and downward erosion would slow where the eroding flow encountered massive sheet lobes and large pillows. A key point is that we are now observing final stages of the process, when everything shut down and froze. Furthermore, melting at the sulfide contact takes place by forming of thin melt film along the contacts of basalt “cores” as described above. Hence, the final stages of erosion of pillowed basalts would be likely to leave behind sharp pillow-shaped contacts, which could give the impression at outcrop observation scale that no melting or erosion had taken place. Interestingly, a published photo (Fig. 8 in Squire et al., 1998) of a basalt pillow on the contact with massive sulfides show similar chromite decorated contacts as described here as the melt-film contact.

5.5. Emulsion textures

Rounded to globular silicates surrounded by sulfide and rounded to globular sulfide surrounded by silicate are frozen examples of emulsions between two melts as described from other lithological environments (Downes, 1989; Naumov et al., 2008; Jakobsen et al., 2011; Valentini et al., 2010) and from other magmatic sulfide deposits (Hawley, 1962). Emulsion textures have been observed on some basal basalt contacts at Victor South-McLeay and Moran but are more common on the sedimentary contacts. Basalt-sulfide emulsion textures are usually found in close proximity to brecciated basalt. The assemblage of textures at Moran is an unusual example of emulsion phase inversion, i.e. from a suspension of silicate liquid droplets in sulfide liquid to the opposite relationship of sulfide liquid droplets in silicate liquid (analogous to mayonnaise, an oil-in-water emulsion, and vinaigrette, water-in-oil). Under most circumstances the suspending liquid in an emulsion is the more abundant one, but this is not always true, and emulsions may invert due to changes in temperature and/or the presence of surfactants (Becher, 1985) through changing the relative surface tensions of the component liquids. The coexistence of inverted emulsions implies that they formed close to the inversion point. The silicate-in-sulfide relationship (Fig. 7a), unusual in magmatic ores in contrast to relatively common “globular ores” where the silicate magma forms the matrix (Barnes et al., 2017b) is thought here to be the result of sulfide melt infiltrating breccias where basalt clasts are completely molten near the sulfide melt. The silicate-in-sulfide inverse emulsion may well be unstable relative to sulfide-in-silicate, but is frozen in during the final stages of the sulfide melt emplacement process before it has time to invert. Other examples of inverted melt emulsions, such as those reported from Sudbury by Hawley (1962) and used by him as one of the first published arguments for a magmatic origin of Ni-Cu sulfide ores, may also provide evidence for an origin in melt films at nearby erosive sulfide liquid-country rock contacts.

5.6. Top-contact chromite

As shown above, chromite commonly develops at basalt-sulfide contacts, but it is unclear why chromite would develop at the contact between massive and matrix ore, where the contact is defined primarily by the presence of cumulus olivine (Groves et al., 1977). Chromite at top contacts is relatively common in komatiite settings

(e.g. Black Swan; Dowling et al., 2004). Patches of ferrichromite beneath the sulfide-komatiite contact can be explained by taking the basalt melt plumes of the basal contact into account. Once these chromite-bearing basalt melt plumes (Fig. 5) exceed the critical size, they detach from the basal contact and float through the sulfide melt into the komatiite melt (Staude et al., 2016). Ferrichromite has a slightly higher density than the sulfide melt (Ewers et al., 1976), but as it usually has silicates attached, especially trapped within the skeletal parts of the crystal, it also floats to the sulfide melt surface. On this contact the much lighter silicate melt detaches from the ferrichromite grains and becomes assimilated by the komatiite melt leaving patches of ferrichromite behind which are still able to float if trapped silicates are situated within the skeletons of the crystal.

An intriguing feature of the top contact samples shown in Figs. 8c and 4 of Staude et al. (2016), is the fine-scale contact-parallel layering in modal proportion of sulfide, chromite and silicate at the contact. A likely explanation for this feature is the operation of a phenomenon that causes similar layering in the size and abundance of vesicles at the tops of lava flows, that of “bubble waves” (Manga, 1996). Where a suspension of buoyant particles (silicate crystals in this case) is floating in a liquid (sulfide melt in this case), particle interaction “traffic jams” in the densely packed parts of the suspension cause ascent rates to slow, while particles in the less dense parts of the suspension interact less with one another and rise faster at Stokes Law velocities. Hence, there is a differential ascent rate between dense and dilute parts of the suspension (A good analogy is with traffic jams on a freeway – cars move slowly within jams, but rapidly between them, causing clusters of clogged traffic separated by free-moving zones). In vesicular lava flows, this process causes the suspension to self-organize into regular layers with a sinusoidal particle (or bubble) density profile (Manga, 1996). The same process causes the upward propagating waves of bubble density observed during the settling of a glass of Guinness beer (Robinson et al., 2008). In the top contact case in Kambalda, the process is further complicated by the tendency of isolated chromite grains to sink relative to silicate grains.

5.7. Embayments: thermomechanical erosion or primary volcanic topography?

The observations reported here, by Staude et al. (2016) and the numerous papers by Leshner and co-workers (cited above) provide strong evidence against the hypothesis of Stone and co-workers (cited above) that the Kambalda ore-hosting embayments are entirely tectonic features. They argued that the embayment and pinchouts can be explained solely by post-magmatic folding and faulting without the need for thermomechanical erosion during the magmatic ore deposition. The existence of plumose melt films, infiltration-melting fronts, vesicular “scum layers” and overall geometry leave little room to doubt that the sulfide melt has eroded laterally into the basalts in the pinchouts. However, a major problem remains in reconciling these observations, the 40 m depth and overall geometry of the Moran embayment with the evidence, summarised by Leshner (1989) and Leshner and Barnes (2009), that the basal contacts of several Kambalda nickel deposits are located stratigraphically entirely on the original basalt lava flow top and apparently not being truncated or eroded by komatiite or sulfide melt (Leshner, 1989). This led to the idea that the embayments itself are pre-magmatic topographic features that are only modified by thermomechanical erosion.

The embayment-hosted massive sulfide orebody at Moran is not located along a basalt flow top and is underlain instead by pillowed basalt, flow-top breccia basalt, and aphanitic basalt (Fig. 2) with clear evidence of melting wherever the contact is not

obscured by shearing. It has also been observed that the sulfides truncate cooling unit surfaces within the pillowed basalt on a low angle in the centre of the deposit (see [Supplementary material](#)). The footwall of Moran is flat (relative to the paleo-horizontal) on a deposit scale, however, especially in the southern part, the basal contact of the embayment is actually slightly convex on a scale of a few metres, with the deepest parts close to the margins of the embayment, as discussed further below. The Long-Moran channel is free of significant amounts of sulfides outside embayments or contains only localized small and thin patches of sulfides (Staude et al., in press). That sulfides were present before the Moran embayment formed is shown by the flanking mineralization that is hosted partly on sediments and partly on basalt, reflecting an early concave embayment where Moran is now situated.

What process can generate, parallel trench-shaped depressions with consistent depth and width and lengths of at least several 10 s of km? Leshner (1983, 1989) proposed a model for the depressions as linear topographic lows developed between parallel adjacent Lunnon Basalt flows flowing down a regional paleo-slope, but the required geometry is not observed on modern shield volcanoes such as Kilauea and Mauna Loa where the “kipukas” between non-overlapping adjacent flows are invariably topographic highs. However, the right type of linear depression is developed in a number of settings within individual flows on the Hawaiian shield volcanoes, most notably as drained lava channels and collapsed lava tubes. In a few cases, such as the extremely long (51 km) 1859 flow on Mauna Loa (Riker et al., 2009) a drained lava channel has approximately the right scale for a Kambalda channel (considering channels as chains of embayments and ore shoots on a length scale of ~10 s of km, as observed between Kambalda and Tramways (Fig. 13). There are no known examples on Hawaiian shield volcanoes where a series of such flows forms multiple parallel linear channels of the right length and width for Kambalda channels. However, drained lava channels appear to be relatively common in modern mid-ocean ridge environments. Soule et al. (2005) report a set of sub-parallel drained channels with segments up to 1 km long, 10–50 m wide and 2–3 m deep in channelized flows on the East Pacific Rise, and Fornari (1986) report collapsed lava tubes of similar width and depth up to 3 km long, also from the East Pacific Rise.

The ore-hosting komatiite lava channels in Kambalda are sub-parallel and can be traced over more than 50 km to the Tramways Group in the south (Gresham and Loftus-Hills, 1981; Marston, 1984). The number of channels is similar in both areas and their direction suggests that they are more or less straight and sub-parallel to the Boulder-Lefroy Fault over the entire distance (Fig. 13). The close parallelism and linear extent is difficult to explain as drained lava channels, but more explicable as reflecting initial fault control.

Brown et al. (1999) suggested that the linear arrangement of the Kambalda embayments reflects control by syn-volcanic grabens, parallel to the major regional Boulder-Lefroy fault, in a geometrical arrangement akin to fissure-swarm fed flows on Iceland (Hjartardottir et al., 2012). If the channels are indeed controlled by primary topographic features in the Lunnon Basalt, then the graben control would have to have been operating at that time, and could potentially have been reactivated during the eruption of the komatiites. Since such faults are not obviously recognizable in mine workings, this model would require that their trace has subsequently been removed by tectonism and/or original thermal erosion. Initial displacements may have been no more than a few metres.

Regardless of whether the primary control on channel and embayment location is related to drained lava channels in the Lunnon Basalt, synvolcanic grabens, or both, we argue on the evidence

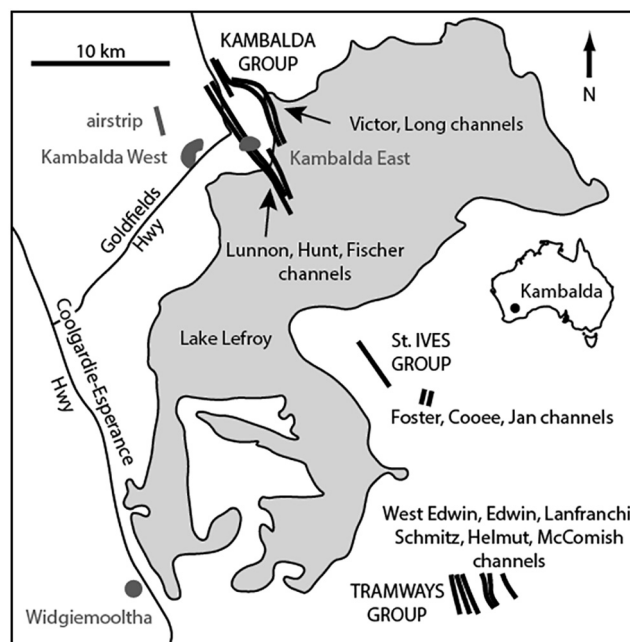


Fig. 13. Map of Kambalda and Lake Lefroy showing komatiite channels (thick black lines) interpreted after Gresham and Loftus-Hills (1981), Marston (1984), Stone and Archibald (2004), and Staude et al. (in press). Approximately 6 channels can be identified in Kambalda and 6 are also found at Lanfranchi in the south spanning a length of nearly straight NNW-SSE komatiite channels of at least 50 km. Areas between Kambalda and St. Ives and between St. Ives and Tramways are unexplored due to a significant depth of the basalt-komatiite contact. The bend in the Kambalda channels is due to the younger dome formation. No further channels have been identified to the west (Marston, 1984) and to the east (Staude et al., in press) of Kambalda. See text for discussion.

presented here that the Moran embayment can be explained by thermomechanical erosion process. Initial sheeted komatiite lava flows were erupted on sea-floor basaltic plains with relatively little regional relief (Squire et al., 1998) and were initially channeled by pre-existing topographic lows dictated by the alignment of the Boulder-Lefroy fault system. Once the channel was established, prolonged flow of komatiite lava started to melt the sedimentary rocks beneath and led to the first accumulation of a Ni-poor sulfide melt in small concave depressions within the channel. Sulfides of this stage of channel formation are preserved as the flanking mineralization to the west and east of Moran. Where sulfide melt was deposited the thermomechanical erosion accelerated due to the low viscosity and high density of the sulfide melt, able to penetrate into the microfractures more easily than komatiite melt, hence increasing the heat transport into the underlying basalt. This self-reinforcing process, aided by localized fragmentation driven by water from the hydrated basalt, deepened the embayment where sulfide melt had been initially deposited, leaving a topographic high of mostly barren channel facies on the flanks and between the embayments.

Once a certain threshold of sulfide and komatiite thickness is reached within the embayment, sulfides became able to melt sideways and undercut the flanks of the embayment, forming pinchouts (Staude et al., 2016). The lateral erosion is driven by the excess pressure within the sulfide melt pool at the lateral basalt contact, this excess pressure being driven by the higher density of both the sulfide melt and the olivine-rich komatiite column within the embayment (Fig. 14). A rough calculation (see Fig. 14 for equations used) gives an excess pressure at the bottom edge of the sulfide melt pool of around 0.2 MPa, assuming a 40 m deep embayment filled with 35 m of olivine-enriched komatiite (with a density of 3200 kg/m³) and a 5 m column of

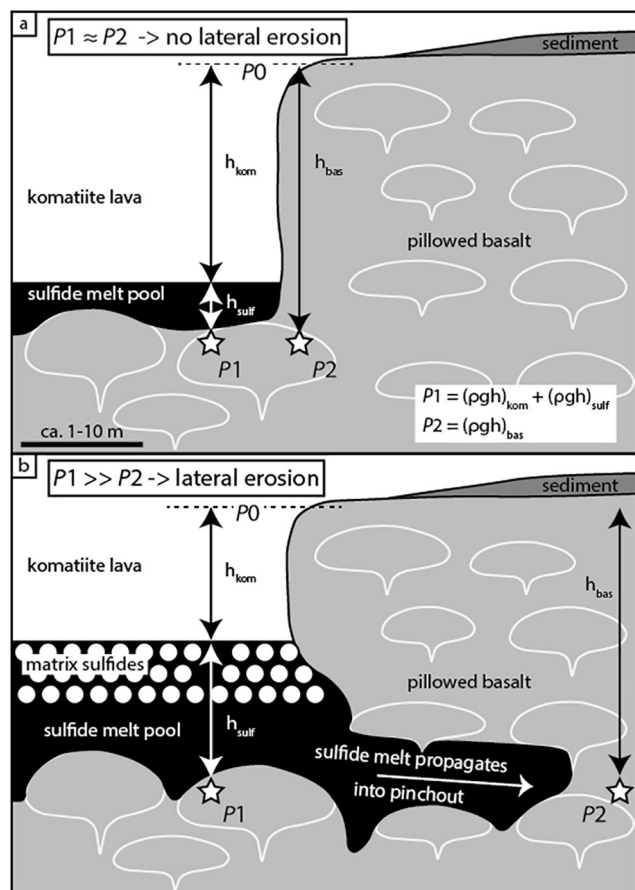


Fig. 14. (A) Cartoon showing the early stage of embayment formation with sulfide melt accumulated at the bottom. The pressure difference between the basalt beneath the embayment and immediately next to the embayment is too low to affect the basalt on the sidewall of the embayment. (B) Cartoon showing an advanced stage of embayment formation. The rising sulfide melt column increases the pressure difference between the basal contact and the immediate basalt on the edge of the embayment. The increase in pressure is accelerated by matrix ore formation as the sulfide liquid increases its height even more. The increasing pressure difference between the basal embayment contact and the basalt on the edge of the embayment forces the sulfides also to melt sideways into the basalt.

massive and matrix sulfide (with a density of 4500 kg/m^3), and a basalt next to the embayment (with a density of 2800 kg/m^3), driving the sulfide melt laterally along original flow contacts as suggested by Leshner (1989). Once the pinchout geometry begins to form, heat from the komatiite is transferred to the floor and roof of the pinchout through the high thermal conductivity of the sulfide liquid, allowing for further melting at the floor and roof of the pinchout and continued lateral propagation. As the komatiite eruption waned the whole system cooled down, freezing the evidence of the final stages of thermomechanical erosion onto the contacts.

An argument raised by Leshner (1989) and others against an erosional origin of embayments is the general flatness (relative to the paleohorizontal) of the embayment floors. At Moran, detailed cross sections (Fig. 3) indicate that the embayment is deeper at its edges, where the thickness of massive sulfide is greater. The sulfide thickness may be explicable by the formation of matrix ores in the centre of the channel, whereby the olivine column sinks partly into the sulfide melt pool due to buoyancy effects, the so-called “billiard ball model” (Naldrett, 1973; Barnes et al., 2017b). The tendency of sulfide liquid at the edge of the pool to erode lateral pinchouts is also likely to contribute to the observed geometry. A further contributing factor may be the flow pattern of lava within the eroding

komatiite flow. In a study of crust formation on open-channel Hawaiian flows, Robertson and Kerr (2012) showed that lava streamlines in an open lava channel cause the hottest lava to follow a helical path with descending flowlines along the outside walls of the flow channel, resulting in more efficient heat transfer and erosion at the edge of the flow rather than in the central part of the floor. Coupled with the pressure-driven lateral erosion effect discussed above and in Staude et al. (2016), this process could account for the characteristic convex-up shape of the base of the Moran embayment.

6. Summary & conclusion

Textural relationships of sulfides with older basalt that reflect thermomechanical erosion processes have been described from the Moran and Victor South-McLeay deposits. All of them contain ferrichromite and include:

1. undulating basal contacts with sulfide-filled microfractures and ferrichromite layers (Figs. 4–7)
2. basalt-sulfide breccia-emulsions on basal contacts (Fig. 4)
3. basalt plumes on basal contacts (Fig. 5)
4. basalt-sulfide emulsions on basal and upper pinchout contacts (Fig. 7)
5. cm-scale silicate-sulfide layering on upper pinchout contacts (Fig. 8)
6. floating vesicular basalt “scum layer” on upper pinchout contacts (Fig. 8)

Textures of sulfides interacting with the basal sedimentary rocks have been observed on the flank of the Moran embayment and are free of ferrichromite and include silicate-sulfide emulsion and MSS cumulates with interstitial Si-rich silicate (Fig. 9).

Textures reflecting thermomechanical erosion processes found on the sulfide-komatiite contact have been observed in most deposits, particularly floating silicate + ferrichromite patches (Fig. 11).

The observed textures indicate that fluids of the hydrated footwall basalt played a major role during the thermomechanical erosion and is evident by vesicular zones trapped underneath the upper level of the pinchout (Staude et al., 2016) and beneath the solid upper crust of the komatiite channel (Beresford et al., 2000). The fluid’s rapid expansion during overheating is responsible for a higher erosion rate as predicted by theoretical calculations (Williams et al., 1998) and our model shows that the entire embayment can be formed by thermomechanical erosion as opposed to the current model assuming an embayment-containing topography is only weakly overprinted by thermomechanical erosion (Leshner, 1989; Williams et al., 1998).

The textures described here reflect different stages of the komatiite lava channel and embayment formation (Fig. 15):

1. The initial lava channel location is dictated by the regional fault set. Channel formation is represented by the Moran flanking sulfides overlying sediments. The komatiite of a thin sheeted flow starts to erode the sediment and accumulates an initial Ni-poor sulfide layer in a concave embayment (Fig. 15a). The thermomechanical erosion process is frozen in place by sediment-sulfide emulsions and sulfide cumulates with interstitial sediment melt.
2. The accumulation of sulfide melt increases the erosion rates due to their very low viscosity and high density, enabling them to fill in the microfractures created by superheated water in the footwall. This led to a faster erosion rate compared to areas without sulfide melt, creating an initial steep sided embayment (Fig. 15b).

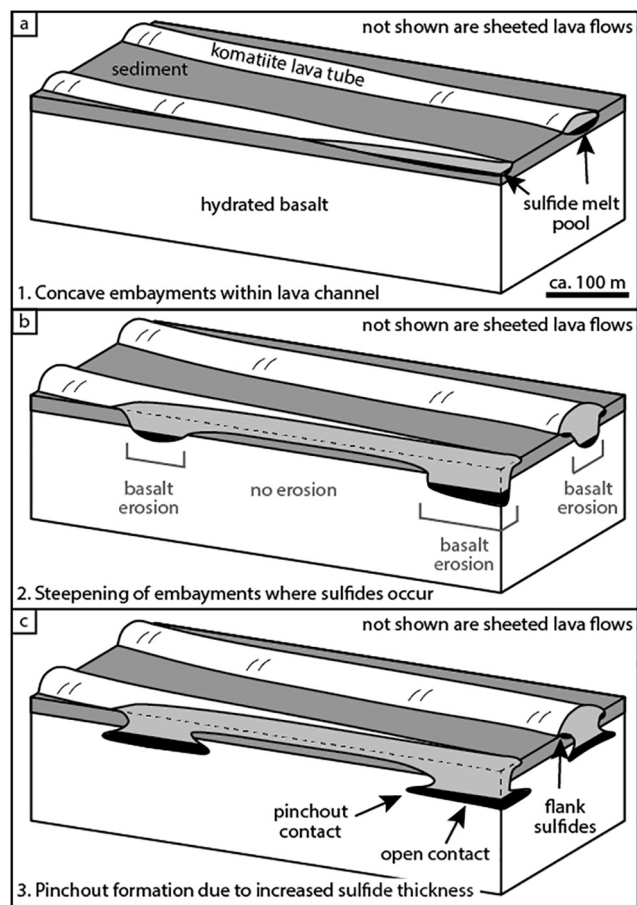


Fig. 15. (A) Cartoon of the initial stage of embayment formation where channelized komatiite lava starts to erode the sediment sporadically within the channel. In these initial concave embayments sulfide melt is able to accumulate. (B) Where sulfide melt accumulated the embayment formation accelerates due to the low viscosity and high density of the sulfide melt (see text for discussion) whereas no significant substrate erosion occurs on sulfide-free parts of the channel. (C) When the sulfide melt thickness reaches a critical height the pressure difference between the underlying basalt in the embayment compared to the basalt next to the embayment increases (see also Fig. 14). This allows the sulfides to also melt their way sideways to create pinchouts.

3. Once a certain threshold of sulfide melt thickness is achieved, the relative pressure variation of the sulfide melt to the adjacent basalt causes the sulfide melt to additionally migrate sideways (Staude et al., 2016) to form a pinchout (Fig. 15c).
4. Decreasing eruption and flow rates and cooling of the komatiite lava freezes the basalt-sulfide contact inside the embayment, preserving the last step of embayment formation.

Acknowledgements

S. Staude is grateful to Independence Group (IGO) for financial support for the analysis and the permission to publish this study. Some samples were provided by Somealy Sheppard and Alex Clark-Hale. Michael Verrall provided assistance with the microbeam XRF mapping. We are thankful to many geologists that worked at Kambalda and improved the understanding and modeling of the deposits and discussions with IGO's Somealy Sheppard, Susan Leeson and Paull Parker as well as Mike Leshar (Sudbury, Canada). Michael Gazley and John Miller (both CSIRO, Perth) are thanked for the review of an early draft. Martin Gole (Perth) and Patrick Hayman (Brisbane) are thanked for critical and constructive

reviews and David Mole and Franco Pirajno for the editorial handling of the manuscript. Steve Barnes and Margaux Le Vaillant are funded by the CSIRO Research Plus Science Leader scheme.

Appendix A. Supplementary data

Supplementary data associated with this article can be found, in the online version, at <http://dx.doi.org/10.1016/j.oregeorev.2017.05.001>.

References

- Barnes, S.J., Gole, M.J., Hill, R.E.T., 1988. The Agnew nickel deposit, Western Australia: Part I. Structure and stratigraphy. *Econ. Geol.* 83, 524–536.
- Barnes, S.J., 2006a. Komatiite-hosted nickel sulfide deposits: geology, geochemistry, and genesis. *Soc. Econ. Geol. Spec. Publ.* 13, 51–118.
- Barnes, S.J., 2006b. Komatiites: petrology, volcanology, metamorphism and geochemistry. *Soc. Econ. Geol. Spec. Publ.* 13, 13–49.
- Barnes, S.J., Beresford, S.W., Le Vaillant, M., 2016a. Interspinifex Ni sulfide ore from the Coronet Shoot, Kambalda: characterisation using microbeam XRF mapping and 3D X-ray computed tomography. *Econ. Geol.* 111, 1509–1517. <http://dx.doi.org/10.2113/econgeo.111.6.1509>.
- Barnes, S.J., Heggie, G.J., Fiorentini, M.L., 2013. Spatial variation in platinum group element concentrations in ore-bearing komatiite at the Long-Victor deposit, Kambalda Dome, Western Australia: enlarging the footprint of nickel sulfide orebodies. *Econ. Geol.* 108, 913–933. <http://dx.doi.org/10.2113/econgeo.108.5.913>.
- Barnes, S.J., Le Vaillant, M., Lightfoot, P.C., 2017a. Textural development in sulfide-matrix ore breccias and associated rocks in the Voisey's Bay Ni-Cu-Co deposit, Labrador. *Ore Geology Reviews*. in review, this volume.
- Barnes, S.J., Mole, D.R., Le Vaillant, M., Campbell, M., Verrall, M., Roberts, M., Evans, N.J., 2016b. Poikilitic textures, heteradcumulates and zoned orthopyroxenes in the Ntaka Ultramafic Complex, Tanzania: implications for crystallisation mechanisms of oikocrysts. *J. Petrol.* 57, 1171–1198. <http://dx.doi.org/10.1093/petrology/egw036>.
- Barnes, S.J., Mungall, J.E., Le Vaillant, M., Godel, B., Leshar, C.M., Holwell, D.A., Lightfoot, P.C., Krivolutsкая, N.A., Wei, B., 2017b. Sulfide-silicate textures in magmatic Ni-Cu-PGE sulfide ore deposits. 1. Disseminated and net-textured ores. *Am. Mineralogist* 102, 473–506. <http://dx.doi.org/10.2138/am-2017-5754>.
- Bavinton, O.A., 1981. The nature of sulfidic sediments at Kambalda and their broad relationships with associated ultramafic rocks and nickel ores. *Econ. Geol.* 76, 1606–1628.
- Bavinton, O.A., Keays, R.R., 1978. Precious metal values from interflow sedimentary rocks from the komatiite sequence at Kambalda, Western Australia. *Geochim. Cosmochim. Acta* 42, 1151–1163.
- Becher, P., 1985. *Encyclopedia of Emulsion Technology*. Marcel Dekker Inc, New York.
- Beresford, S., Cas, R., Lahaye, Y., Jane, M., 2002. Facies architecture of an Archean komatiite-hosted Ni-sulphide ore deposit, Victor, Kambalda, Western Australia: implications for komatiite lava emplacement. *J. Volcanol. Geotherm. Res.* 118, 57–75.
- Beresford, S., Stone, W.E., Cas, R., Lahaye, Y., Jane, M., 2005. Volcanological controls on the localization of the Komatiite-Hosted Ni-Cu-(PGE) Coronet Deposit, Kambalda, Western Australia. *Econ. Geol.* 100, 1457–1467.
- Beresford, S.W., Cas, R.A.F., 2001. Komatiitic invasive lava flows, Kambalda, Western Australia. *Can. Mineral.* 39, 525–535.
- Beresford, S.W., Cas, R.A.F., Lambert, D.D., Stone, W.E., 2000. Vesicles in thick komatiite lava flows, Kambalda, Western Australia. *J. Geol. Soc.* 157, 11–14.
- Brown, M.A.N., Jolly, R.J.H., Stone, W., Coward, M.P., 1999. Nickel ore troughs in Archean volcanic rocks, Kambalda, Western Australia; indicators of early extension. *Geol. Soc. Spec. Publ.* 155, 197–211.
- Cas, R., Self, S., Beresford, S., 1999. The behaviour of the fronts of komatiite lavas in medial to distal settings. *Earth Planet. Sci. Lett.* 172, 127–139.
- Cas, R.A.F., Beresford, S.W., 2001. Field characteristics and erosional processes associated with komatiitic lavas: implications for flow behavior. *Can. Mineral.* 39, 505–524.
- Cowden, A., 1988. Emplacement of komatiite lava flows and associated nickel sulphides at Kambalda, Western Australia. *Econ. Geol.* 83, 436–442.
- Cowden, A., Roberts, D.E., 1990. Komatiite hosted nickel sulphide deposits, Kambalda. In: Hughes, F.E. (Ed.), *Economic Geology of Australia and Papua New Guinea*. Australian Institute of Mining and Metallurgy, Melbourne, pp. 567–581.
- Dowling, S.E., Barnes, S.J., Hill, R.E.T., Hicks, J., 2004. Komatiites and Nickel Sulfide Ores of the Black Swan area, Yilgarn Craton, Western Australia. 2. Geology and genesis of the orebodies. *Miner. Deposita* 39, 707–728.
- Downes, H., 1989. Magma mixing in undersaturated alkaline volcanics, Cantal, Massif Central, France. *Mineral. Mag.* 53, 43–53.
- Evans, D.M., Cowden, A., Barrett, R.M., 1989. Deformation and thermal erosion at the Foster nickel deposit, Kambalda St. Ives, Western Australia. In: Prendergast, M.D., Jones, M.J. (Eds.), *Magmatic Sulphides – The Zimbabwe Volume*. Institute of Mining and Metallurgy, London, pp. 215–219.

- Ewers, W.E., Graham, J., Hudson, D.R., Rolfs, J.M., 1976. Crystallisation of chromite from nickel-iron sulphide melts. *Contrib. Miner. Petrol.* 54, 61–64.
- Ewers, W.E., Hudson, D.R., 1972. An interpretive study of a nickel-iron sulfide ore intersection, Lunnon Shoot, Kambalda. *Econ. Geol.* 67, 1075–1092.
- Fornari, D.J., 1986. Submarine lava tubes and channels. *Bull. Volcanol.* 48, 291–298.
- Frost, K.M., Groves, D.I., 1989a. Magmatic contacts between immiscible sulfide and komatiitic melts; implications for genesis of Kambalda sulfide ores. *Econ. Geol.* 84, 1697–1704.
- Frost, K.M., Groves, D.I., 1989b. Ocellar units at Kambalda: evidence for sediment assimilation by komatiite lavas. In: Prendergast, M.D., Jones, M.J. (Eds.), *Magmatic Sulphides – The Zimbabwe Volume*. Institute of Mining and Metallurgy, London, pp. 207–214.
- Godel, B., Barnes, S.-J., Maier, W.D., 2006. 3-D distribution of sulphide minerals in the Merensky Reef (Bushveld Complex, South Africa) and the J-M Reef (Stillwater Complex, USA) and their relationship to microstructures using X-ray computed tomography. *J. Petrol.* 47, 1853–1872.
- Gole, M.J., Robertson, J., Barnes, S.J., 2013. Extrusive origin and structural modification of the komatiitic Mount Keith Ultramafic Unit. *Econ. Geol.* 108, 1731–1752. <http://dx.doi.org/10.2113/econgeo.108.7.1731>.
- Goscombe, B., Blewett, R.S., Czarnota, K., Groenewald, P.B., Maas, R., 2009. Metamorphic evolution and integrated terrane analysis of the eastern Yilgarn Craton; rationale, methods, outcomes and interpretation. *Geosci. Aust. Rec.* 23, 1–270.
- Gresham, J.J., Loftus-Hills, G.D., 1981. The geology of the Kambalda nickel field, Western Australia. *Econ. Geol.* 76, 1373–1416.
- Groves, D.I., Barrett, F.M., Binns, R.A., McQueen, K.G., 1977. Spinel phases associated with metamorphosed volcanic-type iron-nickel sulfide ores from Western Australia. *Econ. Geol.* 72, 1224–1244.
- Groves, D.I., Korkiakoski, E.A., McNaughton, N.J., Leshner, C.M., Cowden, A., 1986. Thermal erosion by komatiites at Kambalda, Western Australia and the genesis of nickel ores. *Nature* 319, 136–139.
- Hawley, J., 1962. The Sudbury ores, their mineralogy and origin; Part 1, the geological setting. *Can. Mineralogist* 7, 1–29.
- Hjartardottir, A.R., Einarsson, P., Bramham, E., Wright, T.J., 2012. The Krafla fissure swarm, Iceland, and its formation by rifting events. *Bull. Volcanol.* 74, 2139–2153. <http://dx.doi.org/10.1007/s00445-012-0659-0>.
- Houle, M.G., Leshner, C.M., Davis, P.C., 2012. Thermomechanical erosion at the Alexo Mine, Abitibi greenstone belt, Ontario: implications for the genesis of komatiite-associated Ni-Cu-(PGE) mineralization. *Miner. Deposita* 47, 105–128.
- Huppert, H.E., Sparks, R.S.J., 1985. Komatiites I: eruption and flow. *J. Petrol.* 26, 694–725.
- Jakobsen, J.K., Veksler, I.V., Tegner, C., Brooks, C.K., 2011. Crystallization of the Skaergaard intrusion from an emulsion of immiscible iron- and silica-rich liquids: evidence from melt inclusions in plagioclase. *J. Petrol.* 52, 345–373.
- Kauahikaua, J., Cashman, K.V., Mattox, T.N., Heliker, C.C., Hon, K.A., Mangan, M.T., Thornber, C.R., 1998. Observations on Basaltic Lava Streams in tubes from Kilauaea Volcano, Island of Hawaii. *J. Geophys. Res. Solid Earth* 103, 27303–27323.
- Kullerød, G., Yund, R.A., Moh, G.H., 1969. Phase relations in the Cu-Fe-S-Cu-Ni-S and Fe-Ni-S systems. In: Wilson, H.D.B. (Ed.), *Magmatic Ore Deposits*. Economic Geology Monograph, pp. 4323–4343.
- Leshner, C.M., 1983. Localisation and Genesis of Komatiite-Associated Fe-Ni-Cu Sulfide Mineralization of Kambalda, Western Australia (Ph.D.). University of Western Australia, Nedlands, Australia. 318 pages.
- Leshner, C.M., 1989. Komatiite-associated nickel sulfide deposits. In: Whitney, J.A., Naldrett, A.J. (Eds.), *Ore Deposition Associated With Magmas*. Economic Geology Publishing Company, El Paso, pp. 44–101.
- Leshner, C.M., 2007. Ni-Cu-(PGE) deposits in the Raglan area, Cape Smith Belt, New Québec. In: Goodfellow, W.D. (Ed.), *Mineral Deposits of Canada: A Synthesis of Major Deposit-Types, District Metallogeny, The Evolution of Geological Provinces, and Exploration Methods*. St. John's (NL). Geological Association of Canada, Mineral Deposits Division, pp. 351–386.
- Leshner, C.M., Arndt, N.T., Groves, D.I., 1984. Genesis of komatiite-associated nickel sulphide deposits at Kambalda Western Australia: a distal volcanic model. In: Buchanan, D.L., Jones, M.J. (Eds.), *Sulphide Deposits in Mafic and Ultramafic Rocks*. Institute of Mining and Metallurgy, London, pp. 70–80.
- Leshner, C.M., Barnes, S.J., 2009. Komatiite-associated Ni-Cu-(PGE) deposits. In: Li, C., Ripley, E.M. (Eds.), *New Developments in Magmatic Ni-Cu and PGE Deposits*. Geological Publishing House, Beijing, pp. 27–101.
- Manga, M., 1996. Waves of bubbles in basaltic magmas and lavas. *J. Geophys. Res.* B 101, 17457–17465.
- Marston, R.J., 1984. Nickel mineralization in Western Australia. *Geol. Surv. West. Aust. Mineral Resour. Bull.* 14, 271.
- Mungall, J.E., Brenan, J.M., Godel, B., Barnes, S.J., Gailard, F., 2015. Transport of S, Cu and Au in magmas by flotation of sulphide melt on vapour bubbles. *Nat. Geosci.* 8, 216–219. <http://dx.doi.org/10.1038/ngeo2373>.
- Naldrett, A.J., 1973. Nickel sulphide deposits: their classification and genesis, with special emphasis on deposits of volcanic association. *Can. Inst. Min. Metall. Bull.* 66, 45–63.
- Naumov, V.B., Kamenetsky, V.S., Thoams, R., Kononkova, N.N., Ryzhenko, B.N., 2008. Inclusions of silicate and sulfate melts in chrome diopside from the Inagli deposit, Yakutia, Russia. *Geochem. Int.* 46, 554–564.
- Perring, C.S., Barnes, S.J., Hill, R.E.T., 1995. The physical volcanology of komatiite sequences from Forrestania, Southern Cross Province, Western Australia. *Lithos* 34, 189–207.
- Rice, A., Moore, J.M., 2001. Physical modeling of the formation of komatiite-hosted nickel deposits and a review of the thermal erosion paradigm. *Can. Mineral.* 39, 491–503.
- Riker, J.M., Cashman, K.V., Kauahikaua, J.P., Montierth, C.M., 2009. The length of channelized lava flows: insight from the 1859 eruption of Mauna Loa Volcano, Hawaii. *J. Volcanol. Geoth. Res.* 183, 139–156.
- Robertson, J.C., Barnes, S.J., Le Vaillant, M., 2016. Dynamics of magmatic sulphide droplets during transport in silicate melts and implications for magmatic sulphide ore formation. *J. Petrol.* 56, 2445–2472. <http://dx.doi.org/10.1093/petrology/egv078>.
- Robertson, J.C., Kerr, R.C., 2012. Solidification dynamics in channeled viscoplastic lava flows. *J. Geophys. Res.* 117. <http://dx.doi.org/10.1029/2012JB009163>. Citation B07206.
- Robertson, J.C., Ripley, E.M., Barnes, S.J., Li, C., 2015. Sulfur liberation from country rocks and incorporation in mafic magmas. *Econ. Geol.* 110, 1111–1123. <http://dx.doi.org/10.2113/econgeo.110.4.1111>.
- Robinson, M., Fowler, A., Alexander, A., O'Brien, S., 2008. Waves in guinness. *Phys. Fluids* 20, 067101. <http://dx.doi.org/10.1063/1.2929369>.
- Roddick, J.C., 1984. Emplacement and metamorphism of Archaean mafic volcanics at Kambalda, Western Australia – geochemical and isotopic constraints. *Geochim. Cosmochim. Acta* 48, 1305–1318.
- Soule, S.A., Fornari, D.J., Perfit, M.R., Tivey, M.A., Ridley, W.L., Schouten, H., 2005. Channelized lava flows at the East Pacific Rise crest 9–10 degrees N: the importance of off-axis lava transport in developing the architecture of young oceanic crust. *Geochem. Geophys. Geosyst.* 101029/2008GC001954, 6, Q08005: 10.1029/2005GC000912.
- Squire, R.J., Cas, R.A.F., Clout, J.M.F., Behets, R., 1998. Volcanology of the Archaean Lunnon Basalt and its relevance to nickel sulfide-bearing trough structures at Kambalda, Western Australia. *Aust. J. Earth Sci.* 45, 695–715.
- Staude, S., Barnes, S.J., Le Vaillant, M., 2016. Evidence of lateral thermomechanical erosion of basalt by Fe-Ni-Cu sulfide melt at Kambalda, Western Australia. *Geology* (online). <http://dx.doi.org/10.1130/G37977.1>.
- Staude, S., Sheppard, S., Parker, P., Paggi, J., in press. Long-Victor nickel sulfide deposits, Kambalda. *Australian Ore Deposits*, AusIMM Monograph.
- Stone, W.E., Archibald, N.J., 2004. Structural controls on nickel sulphide ore shoots in Archaean komatiite, Kambalda, WA: the volcanic trough controversy revisited. *J. Struct. Geol.* 26, 1173–1194.
- Stone, W.E., Beresford, S.W., Archibald, N.J., 2005. Structural setting and shape analysis of nickel sulfide shoots at the Kambalda Dome, Western Australia: implications for deformation and remobilization. *Econ. Geol.* 100, 1441–1455.
- Swager, C.P., Goleby, B.R., Drummond, B.J., Rattenbury, M.S., Williams, P.R., 1997. Crustal structure of granite-greenstone terranes in the Eastern Goldfields, Yilgarn Craton, as revealed by seismic reflection profiling. *Precamb. Res.* 83, 43–56.
- Thomson, B., 1989. Petrology and stratigraphy of some texturally well preserved thin komatiites from Kambalda, Western Australia. *Geol. Mag.* 126, 249–261.
- Valentini, L., Moore, K.R., Chazot, G., 2010. Unravelling carbonatite-silicate magma interaction dynamics: a case study from the Velay province (Massif Central, France). *Lithos* 116, 53–64.
- Williams, D.A., Kerr, R.C., Leshner, C.M., 1998. Emplacement and erosion by Archaean komatiite lava flows at Kambalda: revisited. *J. Geophys. Res. Solid Earth* 103, 27533–27549.
- Williams, D.A., Kerr, R.C., Leshner, C.M., 2011. Mathematical modeling of thermomechanical erosion beneath Proterozoic komatiitic basaltic sinuous rilles in the Cape Smith Belt, New Quebec, Canada. *Miner. Deposita* 46, 943–958.
- Williams, D.A., Kerr, R.C., Leshner, C.M., Barnes, S.J., 2001. Analytical/numerical modeling of komatiite lava emplacement and thermal erosion at Perseverance, Western Australia. *J. Volcanol. Geoth. Res.* 110, 27–55.